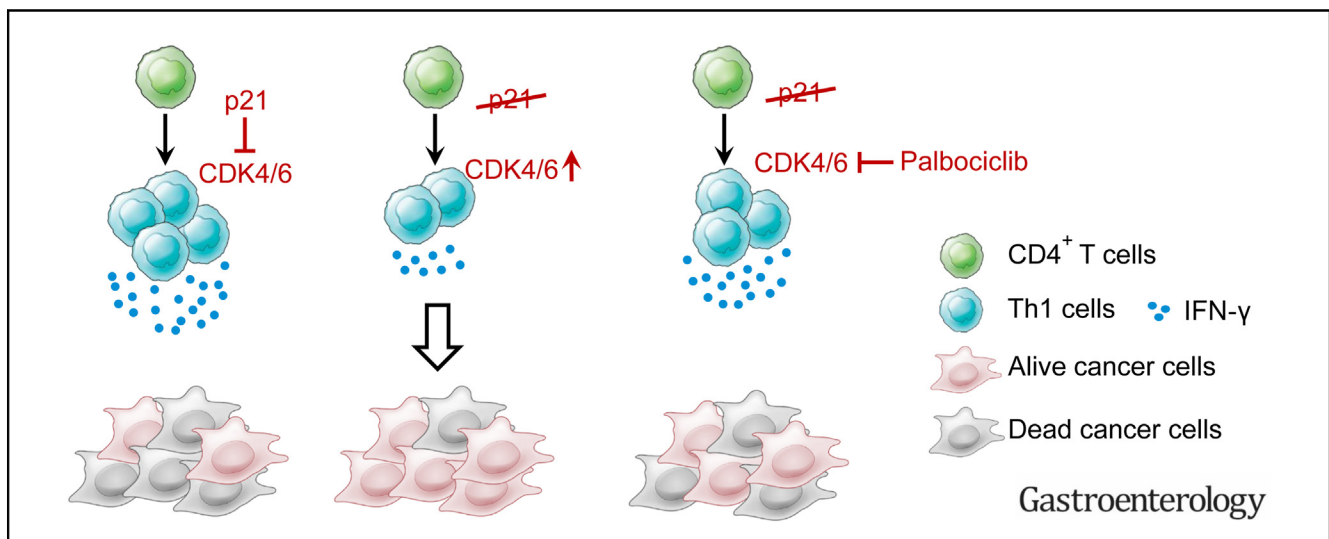# GI CANCER

p21 Prevents the Exhaustion of CD4+ T Cells Within the Antitumor Immune Response Against Colorectal Cancer

Oana-Maria Thoma,[1,2,3] Elisabeth Naschberger,[3,4] Markéta Kubánková,[5] Imen Larafa,[1,2,3] Viktoria Kramer,[1,2,3] Bianca Menchicchi,[1,2,3] Susanne Merkel,[3,6] Nathalie Britzen-Laurent,[3,6] André Jefremow,[1,2,3] Robert Grützmann,[3,6] Kristina Koop,[1,2,3] Clemens Neufert,[1,2,3] Raja Atreya,[1,2,3] Jochen Guck,[5] Michael Stürzl,[3,4] Markus F. Neurath,[1,2,3] and Maximilian J. Waldner[1,2,3,7]

[1]Department of Medicine 1, Friedrich-Alexander-Universität Erlangen-Nürnberg, Erlangen, Germany; [2]German Center for Immunotherapy, Deutsches Zentrum Immuntherapie (DZI), University Hospital Erlangen, Friedrich-Alexander-Universität Erlangen-Nürnberg, Erlangen, Germany; [3]Comprehensive Cancer Center Erlangen-EMN (CCC ER-EMN), Erlangen, Germany; [4]Division of Molecular and Experimental Surgery, Department of Surgery, University Hospital Erlangen, Friedrich-Alexander-Universität Erlangen-Nürnberg, Erlangen, Germany; [5]Max Planck Institute for the Science of Light & Max-Planck-Zentrum für Physik und Medizin, Erlangen, Germany; [6]Department of Surgery, University Hospital Erlangen, Friedrich-Alexander-Universität Erlangen-Nürnberg, Erlangen, Germany; and [7]Erlangen Graduate School in Advanced Optical Technologies (SAOT), Friedrich-Alexander-Universität Erlangen-Nürnberg, Erlangen, Germany

BACKGROUND & AIMS: T cells are crucial for the antitumor response against colorectal cancer (CRC). T-cell reactivity to CRC is nevertheless limited by T-cell exhaustion. However, molecular mechanisms regulating T-cell exhaustion are only poorly understood. **METHODS:** We investigated the functional role of cyclin-dependent kinase 1a (Cdkn1a or p21) in cluster of differentiation (CD) 4+ T cells using murine CRC models. Furthermore, we evaluated the expression of p21 in patients with stage I to IV CRC. In vitro coculture models were used to understand the effector function of p21-deficient CD4+ T cells. **RESULTS:** We observed that the activation of cell cycle regulator p21 is crucial for CD4+ T-cell cytotoxic function and that p21 deficiency in type 1 helper T cells (Th1) leads to increased tumor growth in murine CRC. Similarly, low p21 expression in CD4+ T cells infiltrated into tumors of CRC patients is associated with reduced cancer-related survival. In mouse models of CRC, p21-deficient Th1 cells show signs of exhaustion, where an accumulation of effector/effector memory T cells and CD27/CD28 loss are predominant. Immune reconstitution of tumor-bearing Rag1$^{-/-}$ mice using ex vivo-treated p21-deficient T cells with palbociclib, an inhibitor of cyclin-dependent kinase 4/6, restored cytotoxic function and prevented exhaustion of p21-deficient CD4+ T cells as a possible concept for future immunotherapy of human disease. **CONCLUSIONS:** Our data reveal the importance of p21 in controlling the cell cycle and preventing exhaustion of Th1 cells. Furthermore, we unveil the therapeutic potential of cyclin-dependent kinase inhibitors such as palbociclib to reduce T-cell exhaustion for future treatment of patients with colorectal cancer.

GI CANCER

Colorectal cancer (CRC) is the third most common type of cancer, affecting both men and women.[1] CRC development usually takes several years, and multiple events contribute to its onset.[2] Abnormal cells appear from hyperproliferative cells that continue to accumulate in the epithelial layer. Such cells constantly acquire DNA damage that occurs due to telomere shortening or epigenetic disruptions and manage to escape cell cycle arrest.[3] Mutations in DNA repair and cell cycle arrest genes, such as in the p53/p21 and p16/retinoblastoma (Rb) pathways are frequent and significantly increase the chance that these abnormal cells become cancerogenic.[3,4] Various studies have shown how important p53/p21 and p16/Rb pathway activation is in highly damaged epithelial cells.[5,6]

Furthermore, the evaluation of tumor samples from patients with CRC has shown that p53, p21, and p16 expression in tumor cells significantly improves the outcome.[7,8] This is not surprising, because activation of the p53/p21 and p16/Rb molecular pathways directly inhibits cyclin-dependent kinases (CDKs), such as CDK4 and CDK6, to ensure cell cycle arrest. Surpassing these gate keepers allows tumor cells to proliferate indefinitely. Therefore, current efforts in developing novel CRC treatment focus directly on targeting CDKs, with CDK4/6 inhibitors such as palbociclib now being tested in human clinical trials.[9]

Immune cells constantly shape the tumor microenvironment (TME) in CRC. T cells are especially important players during CRC progression, because high numbers of infiltrating CD3+ cells are often correlated with a positive outcome.[10] T-cell populations in the TME of patients with CRC are, however, highly heterogeneous, varying from functionally active, "bystanders" or even exhausted ones, which can strongly impact the clinical outcome.[11,12] This is due to the constant exposure to tumor antigens, which not only reduces the effector function of T cells but also leads to their exhaustion and senescence induction. The accumulation of exhausted and terminally differentiated effector memory T cells, or so-called TEMRA cells, is often observed in CRC.[13] Exhausted CD8+ T cells are also known to significantly lose CD27/CD28 costimulatory molecules, which can further impede their effector function in CRC.[14] However, whereas CD8+ T-cell dysfunctions are often studied in cancer settings, much less in known about how CD4+ T-cell exhaustion and senescence affect CRC development.

CD4+ T cells are especially important for providing activation signals to CD8+ T cells and further sustain their cytotoxic responses in cancer.[15,16] Interestingly, tumor cells have been shown to be able to induce cellular senescence of CD4+ T cells when they are cocultured for a long period of time.[17] In response to the extensive DNA damage suffered by T cells, they induce cell cycle regulators p53/p21 and p16.[17] p21 activation in CD4+ T cells seems to be especially relevant, because chronically stimulated T cells show high protein expression.[18] Nevertheless, whether p21 function in CD4+ T cells infiltrated in colorectal tumors is detrimental or not is unclear.

WHAT YOU NEED TO KNOW

BACKGROUND AND CONTEXT

T-cell exhaustion impairs the anti-tumor immune response against colorectal cancer. Understanding the molecular mechanisms of cluster of differentiation 4-positive (CD4+) T-cell exhaustion is crucial.

NEW FINDINGS

p21 mediates cell exhaustion of effector CD4+ T cells found in the tumor microenvironment. Palbociclib, an inhibitor of cyclin-dependent kinase 4 and 6, helps restoring loss of function in p21-deficient CD4+ T cells.

LIMITATIONS

Our study unravels the role of p21 in regulating anti-tumor response of CD4+ T cells. Other functions of p21 in T cells remain to be understood.

CLINICAL RESEARCH RELEVANCE

p21 activation is relevant for preventing DNA damage accumulation in highly proliferative, effector CD4+ T cells. In this regard, palbociclib presents great therapeutic potential for improving the anti-tumor response of exhausted T cells in patients with colorectal cancer.

BASIC RESEARCH RELEVANCE

Cell cycle modulation by p21 plays an important role in the effector function of T cells. Evaluation of other molecules involved in the cell cycle machinery may provide a better understanding of mechanisms leading to T-cell exhaustion in colorectal cancer.

To answer this question, we have used azoxymethane/dextran sodium sulfate (AOM/DSS) and murine carcinoma (MC38) orthotopic models in Rag1$^{-/-}$ mice reconstituted with wild-type or p21-deficient CD4+ T cells. We evaluated the effector function of p21$^{-/-}$ CD4+ T cells as well as maturation status and CD27/CD28 expression, in response to CRC tumors. Most importantly, we showed that p21 nuclear expression in CD4+ T cells is especially relevant in tumors from patients with CRC.

Materials and Methods

A detailed description of the methods used in the study can be found in the Supplementary Materials and Methods.

Most current article

Human Tissue

Human colon cancer samples were taken according to Ethical Committee approval from 95 patients who underwent primary tumor resection at the University Hospital Erlangen between September 2007 and October 2020, with various stages of CRC (n = ≥18 samples/stage). The clinical details of the patients can be found in Supplementary Table 1. The immunostaining protocol and staining quantification procedure is described in the Supplementary Materials and Methods.

In Vivo Colorectal Cancer Models

The in vivo models were done according to the State Government of Middle Franconia Institutional Animal Care and Use Committee. MC38 and AOM/DSS models were performed on 8- to 15-week-old male or female immune-deficient $Rag1^{-/-}$ mice (The Jackson Laboratory). $Cdkn1a^{-/-}$ ($p21^{-/-}$) and C57BL/6J (B6/J) mice were used as donor animals for the in vivo experimental tumor models (AOM/DSS and MC38 orthotopic tumor models) in $Rag1^{-/-}$ mice as well as for the in vitro studies. All knockout mice had a B6/J background and have been previously described in the literature.[19,20] The tumor models were performed as previously described in literature.[21,22] A detailed description of each model can be found in the Supplementary Materials and Methods. The overall well-being of the mice was periodically assessed via endoscopy (Coloview system, Karl Storz) and scored by using the murine endoscopic index of colitis severity and a general score for tumor growth.[23]

In Vitro Cell Culture Models

For the in vitro type 1 helper T cells (Th1), polarization of naïve $CD4^+CD25^-$ cells were isolated from B6/J and $p21^{-/-}$ spleens (Miltenyi Biotec) and stimulated for 5 days using anti-CD3/anti-CD28, interleukin (IL) 12 and α-IL4. Female and male mice were both used for in vitro models. The cells were cultured in RPMI medium (Sigma-Aldrich), with 10% fetal bovine serum (Gibco) and 1% penicillin/streptomycin (Sigma-Aldrich). Th1 polarization of B6/J cells was tested using a p21 inhibitor (UC2288, Abcam) treatment added 2 days after cell stimulation.

For palbociclib experiments, $p21^{-/-}$ Th1 cells were stimulated with various concentrations of palbociclib (Selleckchem) on day 2. In coculture experiments, palbociclib-treated and untreated Th1 cells were added to MC38 cells for 24 hours in a 10:1 concentration. A list of the reagents and their dilutions can be found in Supplementary Table 2.

Flow Cytometry Analysis

Immune cells isolated from blood, mesenteric lymph nodes (mLNs), spleens, tumors, and in vitro stimulations were analyzed by using flow cytometry. The detailed staining can be found in the Supplementary Materials and Methods.

The telomere length assay was based on a flow–fluorescence in-situ hybridization protocol.[24] The cells were resuspended in formamide (Sigma-Aldrich), with or without the peptide nucleic acid–fluorescence in-situ hybridization probe (Panagene). Propidium iodide staining solution (Invitrogen) was used to allow cell cycle detection. A list of all the antibodies used can be found in Supplementary Table 3.

Real-Time Fluorescence Deformability Cytometry

For high-throughput 1-dimensional fluorescence imaging of cells using real-time fluorescence deformability cytometry (RT-FDC), the cells were prepared as following: Cell Tracker Deep Red Dye was used for cytoplasmic staining and Ki67 for nuclear staining. Then, the cells were incubated with p21 (Boster), followed by Alexa Fluor 488 donkey anti-rabbit secondary antibody immunoglobulin G (BioLegend). Single staining was used for RT-FDC color compensation. RT-FDC measurements were performed as described previously.[25]

Statistical Analysis

The data were analyzed by using GraphPad Prism 8 software (GraphPad Software). For column analysis, the unpaired 2-tailed t test or 1-way analysis of variance with Tukey's correction was used. For grouped analysis, 2-way analysis of variance with Šidák's correction was used. Curves were plotted by using a simple linear regression model, and r values were calculated with the parametric Pearson's correlation. Statistical differences are indicated as follows: $*P \leq .05$, $**P \leq .01$, $***P \leq .001$, $****P \leq .0001$.

Results

p21 Deletion in $CD4^+$ T Cells Influences Colorectal Cancer Development Independent of Cytotoxic $CD8^+$ T Cells

We evaluated p21 expression in $CD4^+$ T cells infiltrated in murine CRC using tumor sections from wild-type B6/J mice that were subjected to the orthotopic MC38 or AOM/DSS model. Immunohistochemistry results showed that $CD4^+$ T cells in the TME have cytoplasmic and nuclear p21 expression (Figure 1A and Supplementary Figure 1A).

To evaluate the functional role of these cells, we reconstituted $Rag1^{-/-}$ mice with B6/J or $p21^{-/-}$ $CD4^+$ T cells and subjected them to the MC38 model (Figure 1B). Mice that received $p21^{-/-}$ $CD4^+$ T cells developed significantly bigger tumors than those injected with control $CD4^+$ T cells (mean 3.650 vs 1.889) (Figure 1C and D). Surprisingly, a significant increase in tumor growth was observed even in $Rag1^{-/-}$ mice injected with a mixture of B6/J $CD8^+$ T cells and p21-deficient $CD4^+$ T cells (Supplementary Figure 1B–D). Similarly, $Rag1^{-/-}$ mice exposed to the AOM/DSS model and reconstituted with $p21^{-/-}$ $CD4^+$ T cells had significantly increased tumor burden compared with those receiving wild-type $CD4^+$ T cells (Supplementary Figure 1E–H), despite the cotransfer of wild-type $CD8^+$ T cells.

Cleaved-caspase-3 staining revealed that tumor cells from $Rag1^{-/-}$ mice injected with $p21^{-/-}$ $CD4^+$ T cells were less apoptotic than those from control mice ($P = .0311$) (Figure 1E). No significant changes have been observed regarding tumor cell proliferation (Figure 1F), whereas tumor vessel density was modestly increased in mice
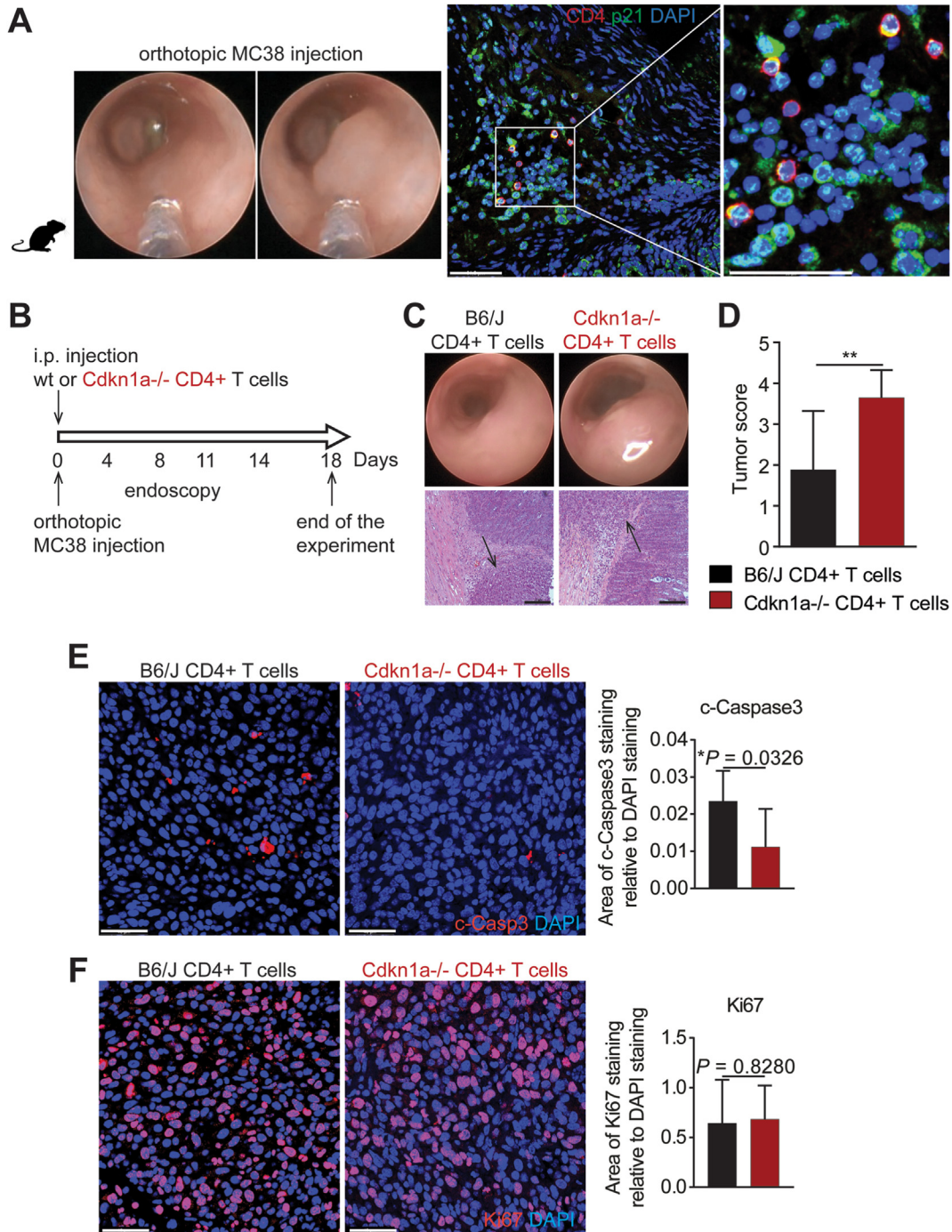
Figure 1. p21 deletion in CD4+ T cells leads to increased tumor growth in the MC38 orthotopic tumor model by mediating tumor cell death. (*A*) MC38 orthotopic model in B6/J mice and immunohistochemistry images show p21 expression in CD4+ T cells infiltrated in the TME (scale bar = 50 μm). (*B*) Schematic representation of the MC38 orthotopic model used for Rag1$^{-/-}$ mice that received B6/J or Cdkn1a$^{-/-}$ CD4+ T cells intraperitoneally (i.p.). (*C*) Endoscopy and H&E staining on tumor tissue from Rag1$^{-/-}$ mice reconstituted with B6/J or Cdkn1a$^{-/-}$ CD4+ T cells (scale bar = 100 μm). (*D*) Tumor growth assessment as determined by endoscopic scoring (at *t* = 18 days after MC38 injection, n = $\geq$9 mice/group). Tumor cell death and proliferation assessment by immunohistochemistry staining for (*E*) cleaved caspase-3 (c-Caspase3) and (*F*) Ki67 (n = $\geq$6 samples/group). Cell nuclei were counterstained with 4′,6-diamidino-2-phenylindole (DAPI) (scale bar = 50 μm). The data are shown as the mean ± standard deviation. Significant differences are observed using 2-tailed unpaired *t* test. *$P \leq$ .05, **$P \leq$ .01.

receiving p21-deficient CD4+ T cells (Supplementary Figure 2*A*). Although the infiltration of CD3+ T cells and macrophages in the TME remained unchanged, the numbers of neutrophils in the TME were decreased in Rag1$^{-/-}$ mice reconstituted with Cdkn1a$^{-/-}$ CD4+ T cells (Supplementary Figure 2*B–D*).
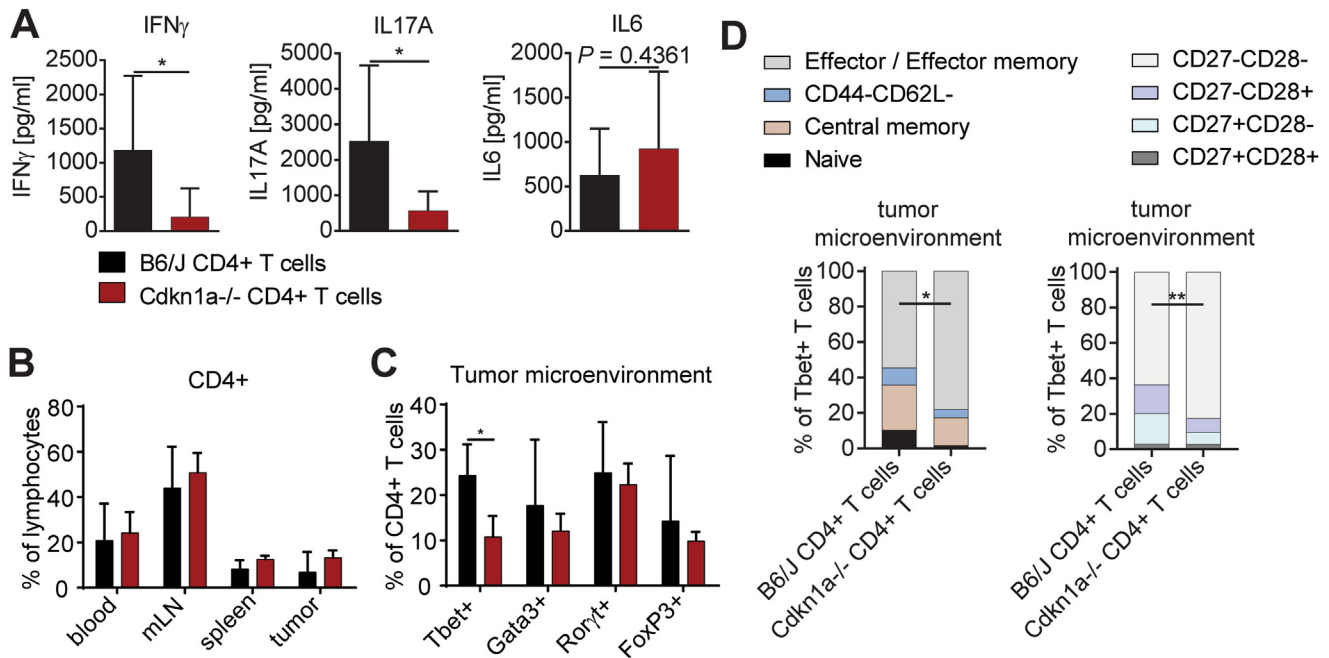
Figure 2. Effector function characterization of CD4$^+$ T cells lacking p21 in the TME. (*A*) IFNγ, IL17A, and IL6 protein expression of immune cell infiltrates in the TME of control and knockout mice (n = $\geq$5 samples/group). (*B*) Flow cytometry data show CD4$^+$ T-cell relative numbers in the blood, mLNs, spleen, and TME of the Rag1$^{-/-}$ mice reconstituted with B6/J or Cdkn1a$^{-/-}$ CD4$^+$ T cells (n = $\geq$7 samples/group). (*C*) The immune cells from TME were stained for specific transcription factor markers to describe their polarization status (n = $\geq$7 samples/group). (*D*) Maturation status of wild-type and p21-lacking Tbet$^+$ T cell as shown by fluorescence-activated cell sorter staining for CD44 and CD62L as well as for CD27 and CD28 costimulatory molecules (n = $\geq$5 samples/group). The data are shown as the mean $\pm$ standard deviation. Significant differences are observed by using 2-tailed unpaired *t* test or 2-way analysis of variance corrected with Šidák's multiple comparison test. *$P \leq$ .05, **$P \leq$ .01.

Loss of p21 in CD4$^+$ T Cells Leads to Reduced Numbers of T-Box Transcription Factor-Positive Cells Infiltrated Into the Tumor Microenvironment

We further investigated the cytokine expression of immune cells isolated from the TME. Enzyme-linked immunosorbent assay measurements from protein lysates showed significantly decreased interferon (IFN)-γ (P = .0396) and IL17A (P = .0128) expression in Rag1$^{-/-}$ mice that received p21$^{-/-}$ CD4$^+$ T cells compared with the controls, whereas IL6 cytokine expression remained unchanged (Figure 2*A*).

Although the overall numbers of CD4$^+$ T cells in the blood, mLNs, spleen, or TME and total number of live cells in the TME were comparable between both groups (Figure 2*B* and Supplementary Figure 2*E*), p21 deficiency resulted in decreased relative numbers of T-box transcription factor-positive (Tbet$^+$) cells infiltrated in the TME (Figure 2*C* and Supplementary Figure 2*F* and *G*). Similarly, fewer Tbet$^+$ CD4$^+$ T cells were observed in Rag1$^{-/-}$ mice reconstituted with control CD8$^+$ T cells and Cdkn1a$^{-/-}$ CD4$^+$ T cells and exposed to the AOM/DSS model (Supplementary Figure 2*H* and *I*).

In CRC, constant exposure to tumor antigens can lead to increased numbers of terminally differentiated memory T cells.[26] Therefore, we evaluated the numbers of naïve and memory CD4$^+$ T cells found in the TME. Interestingly, p21 deficiency in Tbet$^+$ T cells led to a significant increase in

relative numbers of effector/effector memory cells (Figure 2*D* and Supplementary Figure 2*G*). Furthermore, p21$^{-/-}$ Tbet$^+$ CD4$^+$ T cells in the TME showed a predominantly exhausted phenotype compared with the wild-type Tbet$^+$ CD4$^+$ T cells (Figure 2*D* and Supplementary Figure 2*J*).

p21 Nuclear Expression Is Necessary for Th1 T-Cell Polarization and Protects Against T-Cell Exhaustion

To evaluate the functional role of p21 during Th1 cell polarization, we performed several in vitro models. Time-dependent in vitro experiments revealed that p21 is expressed as early as day 2 of activation (naïve Th cells) and Th1 polarization, remained constant over the following 3 days of stimulation (Figure 3*A*), and was mainly located in the nucleus (Figure 3*B*).[25]

Furthermore, p21-deficient CD4$^+$ T cells polarized significantly less in Th1 cells with decreased relative numbers of IFNγ^+ cells and reduced cytokine production (Figure 3*C* and *D* and Supplementary Figure 3*B*). Interestingly, p21-inhibition with UC2288 in Th1 cells revealed a decrease of IFNγ^+ production in a concentration-dependent manner (Supplementary Figure 3*A* and *B*). To test for sex differences, we performed individual in vitro experiments using male and female mice. Significantly fewer p21-deficient CD4$^+$ T cells polarized in Th1 cells compared with
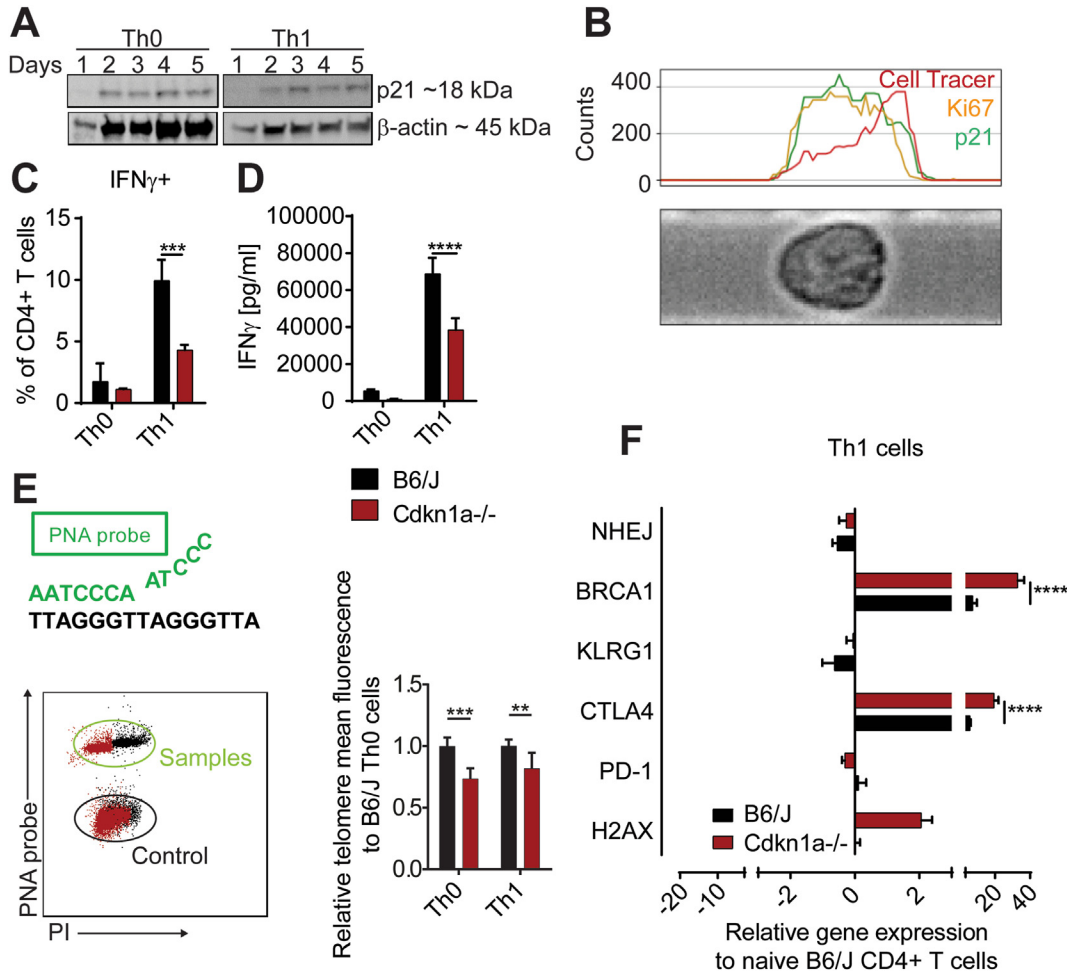
Figure 3. p21 nuclear activation influences in vitro T-cell activation and Th1 polarization and protects against their exhaustion. (*A*) Western blot analysis of time-dependent p21 protein expression in naïve Th cells (Th0) and Th1 cells from B6/J mice. (*B*) RT-FDC measurements on in vitro Th1 cells (*t* = 3 days) show nuclear location of p21 (n = 500 cells). (*C*) Relative numbers of IFNγ$^+$ T cells after 5 days of in vitro T-cell polarization. (*D*) Enzyme-linked immunosorbent assay measurements show IFNγ production in Th1 polarized cells from B6/J and p21$^{-/-}$ mice (n = 3 replicates/group, from 3 independent experiments). (*E*) Flow cytometric measurements of telomere mean fluorescence of Th0 and Th1 cells from control and knockout mice (n = ≥5 samples/group from 2 different experiments). (*F*) Relative gene expression in Th1 cells from B6/J and Cdkn1a$^{-/-}$ mice related to cell repair, senescence, exhaustion, and DNA damage, as shown by quantitative real-time polymerase chain reaction data (n = 3 replicates/group). The data are shown as the mean ± standard deviation. Significant differences are observed using 2-way analysis of variance corrected with Šidák's multiple comparison test. **$P \leq .01$, ***$P \leq .001$, ****$P \leq .0001$.

control cells, independent of the sex (Supplementary Figure 3*C*).

p21 loss further reduced the relative numbers of central memory (CD62L$^+$CD44$^+$) cells and increased the numbers of effector/effector memory (CD62L$^-$CD44$^+$) cells (Supplementary Figure 3*D*). A significant decrease in the relative numbers of CD27$^+$CD28$^+$ T cells was also predominant in p21-deficient Th1 cells (Supplementary Figure 3*E*).

After activation, T cells commonly lose CD27 and CD28 as they extensively proliferate.[27] Because p21 is directly related to the cell cycle, we investigated whether its loss might directly affect proliferation and cell death. Indeed, p21 deletion in CD4$^+$ T cells significantly affected T-cell proliferation, whereas cell death was unaffected (Supplementary Figure 3*F–H*). The extensive

proliferation of p21-deficient Th1 cells was accompanied by increased telomere loss (Figure 3*E*) and an upregulation of genes related to exhaustion (cytotoxic T lymphocyte-associated protein [*CTLA4*]), DNA damage (histone family member X [*H2AX*]), and repair (breast cancer type1 susceptibility protein [*BRCA1*]), as shown in Figure 3*F*.

Th1 T Cells Lacking p21 Show Reduced Cytotoxic Potential Against MC38 Cells

The decrease in Tbet$^+$ T cells and IFNγ cytokine production, together with significantly less tumor cell death observed in Rag1$^{-/-}$ injected with p21-deficient CD4$^+$ T cells, suggest that p21 loss in Th1 cells might reduce their cytotoxic effect. We evaluated this hypothesis by using in vitro Th1/MC38 coculture models (Figure 4*A*). In vitro
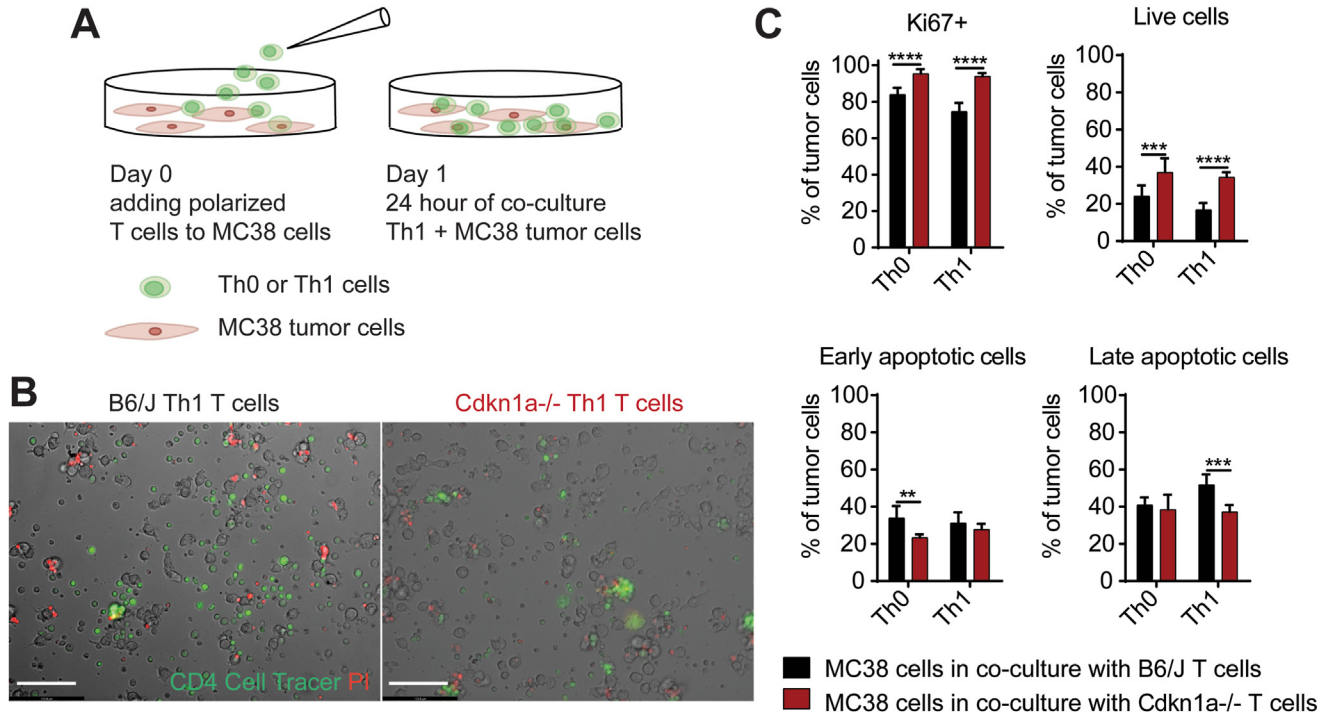
Figure 4. Cytotoxic function of p21-deficient Th1 cells. (*A*) Schematic representation of the MC38-Th1 T-cell coculture experiments. Th0, naïve T-helper cells. (*B*) Propidium iodide (PI) staining shows tumor cell death in the coculture experiments (scale bars = 50 μm). (*C*) Fluorescence-activated cell sorter data shows MC38 tumor cell proliferation and cell death after in vitro coculture with B6/J or Cdkn1a$^{-/-}$ Th1 polarized T cells (n = $\geq$6 replicates/group from 3 independent experiments). The data are shown as the mean $\pm$ standard deviation. Significant differences are observed using 2-way analysis of variance corrected with Šidák's multiple comparison test. **$P \leq$ .01, ***$P \leq$ .001, ****$P \leq$ .0001.

polarization generated significantly fewer IFNγ^+ T cells due to p21 loss in CD4$^+$ T cells (Supplementary Figure 4*A* and *B*). Furthermore, p21-deficient Th1 cells showed reduced cytotoxic capacities against MC38 cells (Figure 4*B* and *C* and Supplementary Figure 4*C*).

Palbociclib, a Cyclin-Dependent Kinases 4/6 Inhibitor, Can Restore p21 Deficiency in Th1 T-Cell Polarization

p21 activation in cells can directly interfere with the cell cycle, being a marker of cellular senescence induction.[5] Because B6/J Th1 cells continue to proliferate, even after p21 activation, we hypothesized that its role in such early time points during polarization might be necessary to ensure proper gene and protein transcription during cell cycle growth phase 1 (G$_1$). Time-dependent analysis of cell cycle showed that p21 loss in CD4$^+$ T cells significantly decreased the relative numbers of cells in quiescent state (G$_0$)/G$_1$ phase, from 53.17% to 46.60%, as early as 48 hours of stimulation (Figure 5*A*). Furthermore, the relative numbers of cells in the synthesis phase were significantly increased in Th1 cells lacking p21 compared with the wild-type cells. After 72 hours, the numbers of cells in G$_2$/mitotic phase in p21$^{-/-}$ Th1 cells were also decreased. Interestingly, the change in the relative numbers of cells in G$_0$/G$_1$ phase in p21-deficient Th1 cells appears to affect the relative numbers of IFNγ^+ T cells (*P* $\leq$ .0001), but not Tbet$^+$ ones, compared with the B6/J Th1

cells (Figure 5*B*), suggesting proper polarization but reduced effector function.

The direct mechanism through which p21 interferes with cell cycle in the G$_0$/G$_1$ cell cycle phase is based on inhibiting CDK2 and CDK4/6.[28,29] Therefore, we attempted to restore the phenotype by targeting CDK4/6, using common CDK4/6 inhibitors such as palbociclib, ribociclib, and abemaciclib.[9,30] Interestingly, palbociclib and ribociclib significantly increased the numbers of IFNγ^+ T cells and IFNγ cytokine production in p21$^{-/-}$ CD4$^+$ T cells, but abemaciclib did not have any effect or even worsened IFNγ production (Supplementary Figure 5*A*). Among all, abemaciclib completely inhibits the phosphorylation of the Rb protein, stopping cell cycle and inducing an increased rate of cell death (Supplementary Figure 5*B*, *C*, and *E*). Therefore, lack of effect of abemaciclib in restoring the number of p21$^{-/-}$ IFNγ^+ T cells might be the result of predominant cell death observed during the treatment.

When comparing B6/J and p21$^{-/-}$ Th1 cells, with or without treatment, we observed that palbociclib significantly increased the relative IFNγ numbers in p21-deficient Th1 cells (from 4.88% to 11.60%), without affecting control cells (Figure 5*C*). Ribociclib could also partially restore p21$^{-/-}$ Th1 polarization (Supplementary Figure 5*D*). An improvement in the relative cell numbers in G$_0$/G$_1$ cell cycle was also noticeable in p21$^{-/-}$ Th1 cells (Figure 5*D*). Last, palbociclib also restored the effector/effector memory and central memory phenotype while protecting against CD28 loss (Figure 5*E*).
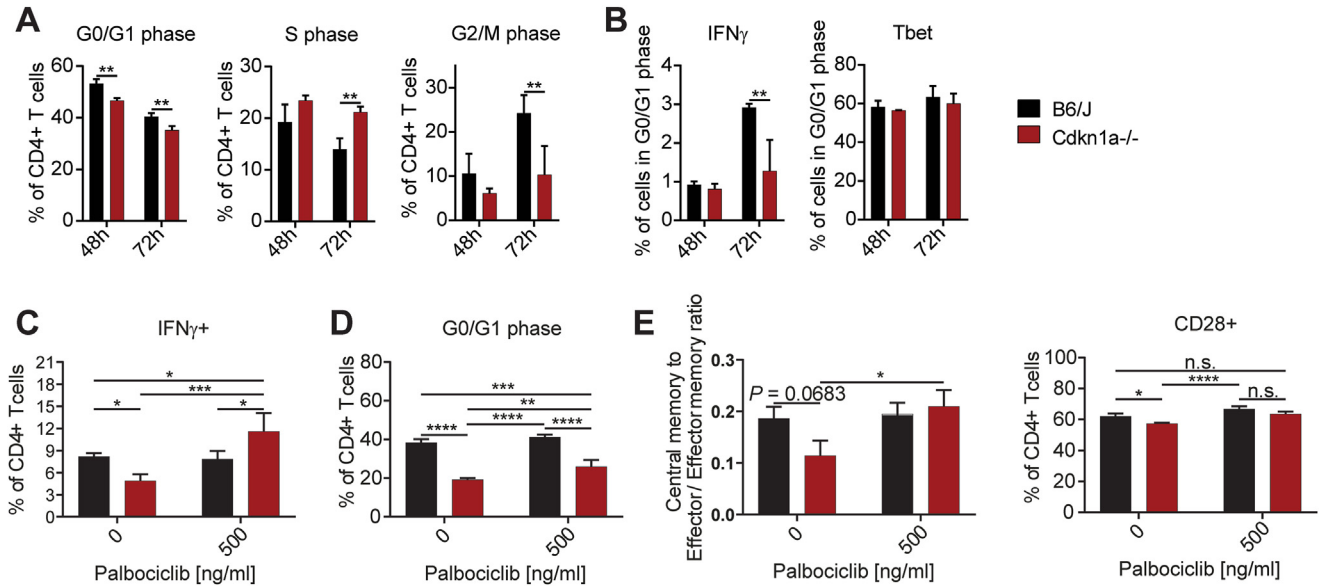
Figure 5. p21 influences gene expression during G_0/G_1 cell cycle phase in Th1-polarized T cells. (*A*) Time-dependent cell cycle and (*B*) Tbet$^+$ and IFNγ^+ during G_0/G_1 phase analysis of wild-type and Cdkn1a$^{-/-}$ Th1 cells as shown by flow cytometry (n = 3 replicates/group). (*C*) Relative number of IFNγ-expressing Th1 cells and (*D*) Th1 cells in G_0/G_1 phase from B6/J and Cdkn1a$^{-/-}$ mice after palbociclib treatment. (*E*) Maturation status and CD28 expression of Th1 cells from B6/J and Cdkn1a$^{-/-}$ in response to palbociclib treatment. The treatment experiments were performed twice with n = 3 replicates/experiment. The data are shown as the mean ± standard deviation. Significant differences are observed using 2-way analysis of variance corrected with Šidák's multiple comparison test. *$P \leq .05$, **$P \leq .01$, ***$P \leq .001$, ****$P \leq .0001$.

Palbociclib-Treated p21$^{-/-}$ Memory CD4$^+$ T Cells Show Increased Cytotoxic Potential

Because CDK4/6 inhibition using palbociclib restored the IFNγ cytokine production, it might be helpful in assisting with the Th1 cytotoxic function against MC38 cells as well. We further cocultured palbociclib-treated and untreated Th1 cells from B6/J and p21$^{-/-}$ mice with MC38 cells (Figure 6*A*). Palbociclib-treated Cdkn1a$^{-/-}$ Th1 cells behaved similar to untreated and treated B6/J Th1 cells in inducing MC38 tumor cell death and were able to induce more cell death compared with the untreated p21$^{-/-}$ Th1 cells (Figure 6*A* and *B* and Supplementary Figure 5*F*).

We also evaluated whether such a phenotype can be observed in the in vivo MC38 orthotopic model. A schematic representation of the generated model is displayed in Figure 6*C*. In short, we generated memory CD4$^+$CD44$^+$ T cells by exposing p21$^{-/-}$ mice to the MC38 orthotopic model. After 3 weeks, the cells were collected from spleens and mLNs of these mice and activated in vitro for 24 hours. Before these cells were injected into Rag1$^{-/-}$ mice bearing MC38 tumors, some were exposed to palbociclib for 15 minutes. Tumor growth was then monitored for 12 days (Figure 6*D*). Decreased tumor growth in Rag1$^{-/-}$ mice reconstituted with palbociclib-treated CD4$^+$CD44$^+$ T cells was observed as early as day 7 after injection. TME analysis of immune-cell infiltration revealed a trend for increased Tbet$^+$ T-cell infiltration (31.10% compared with 21.72% in control mice) (Figure 6*E*), with no change in total numbers of live cells (Supplementary Figure 5*G*).

Low p21 Expression in CD4$^+$ T Cells Found at the Tumor Site Affects Cancer-Related Survival of Patients With Colorectal Cancer

Last, we investigated whether p21 expression might have a prognostic value as well. CD4 and p21 staining on samples from patients with CRC (stage I to IV) revealed that p21 is expressed in the nucleus and cytoplasm of CD4$^+$ T cells to a certain degree (Figure 7*A*). These results are similar to what we initially observed in B6/J mice exposed to both orthotopic MC38 and AOM/DSS models.

We further evaluated how cytoplasmic and nuclear p21 expression is modulated in patients with stage I to IV CRC. The expression of p21 was quantified by using a cytoplasmic and nuclear region of interest in randomly chosen p21-expressing CD4$^+$ T cells (Figure 7*B*). Interestingly, p21 cytoplasmic expression remained unchanged independent of CRC stage, and p21 nuclear expression is reduced in the stages late III to IV compared with stage I (mean value stage I: 137.80, stage II: 132.80, stage III: 97.62, and stage IV: 91.79). Similarly, nuclear/cytoplasmic ratio in stage I to IV CRC showed a negative correlation ($r = -0.05395$, $P < .0001$).

Based on these results, we set out to find whether low or high p21 expression could change cancer survival in CRC patients. Based on an area under the receiver operating characteristic curve of 0.798 (95% confidence interval, 0.62–0.83; $P = .0001$), we used 113.2 mean fluorescence as a threshold for p21 nuclear mean fluorescence (Figure 7*C*). Kaplan-Meyer survival curves revealed that patients with low p21 nuclear expression in CD4$^+$ T cells have decreased cancer-related survival compared with those that have high
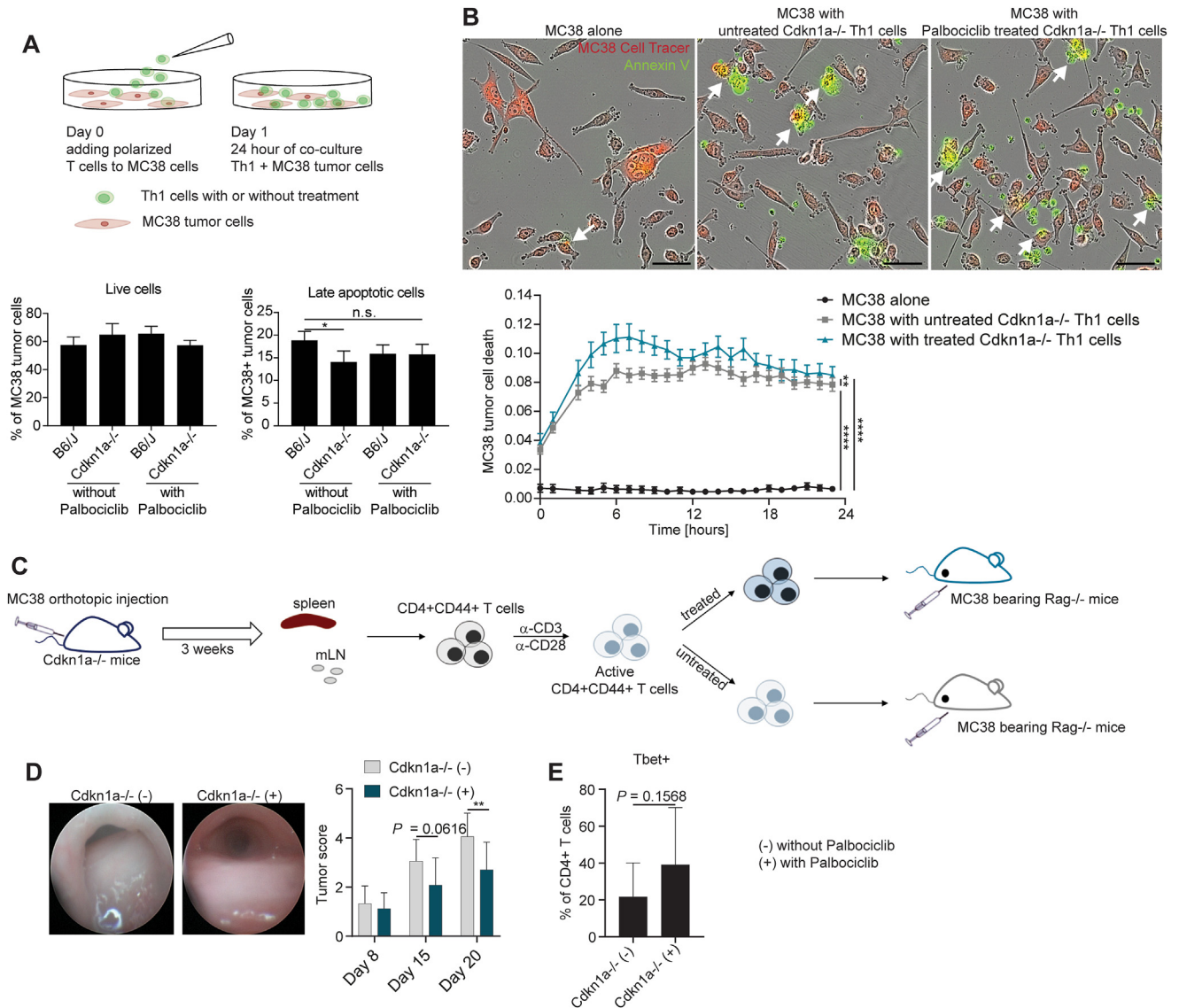
Figure 6. Cytotoxic function of p21-deficient memory CD4$^+$CD44$^+$ T cells can be restored by palbociclib treatment. (*A* and *B*) MC38 tumor cell death after coculture with in vitro stimulated- and palbociclib-treated Th1 cells from B6/J and Cdkn1a$^{-/-}$ mice, as shown by flow cytometry data (n = ≥4 replicates/group) and Incucyte (Sartorius) measurements (n = 7 replicates/group). (*C*) In vivo MC38 orthotopic model using p21$^{-/-}$ memory CD4$^+$CD44$^+$ T cells treated with palbociclib. (*D*) Endoscopy shows tumor growth in Rag1$^{-/-}$ mice reconstituted with untreated (−) or palbociclib-treated (+) Cdkn1a$^{-/-}$ memory T cells (n = ≥9 mice/group from 3 different experiments). (*E*) Relative number of Tbet$^+$ T cells found at the tumor site in Rag1$^{-/-}$ mice reconstituted with untreated (−) and palbociclib-treated (+) CD4$^+$CD44$^+$ T cells (n = ≥9 samples/group from 3 different experiments). The data are shown as the mean ± standard deviation. Significant differences are observed by using 2-tailed unpaired *t* test, 1-way analysis of variance corrected with Tukey's multiple comparison test, or 2-way analysis of variance corrected with Šidák's multiple comparison test. *$P ≤ .05$. **$P ≤ .01$, ****$P ≤ .0001$.

p21 expression ($P = .027$) (Figure 7*D*). This suggests that p21 nuclear expression in CD4$^+$ T cells might be useful as a prognostic marker in patients with CRC.

Discussion

CDK inhibitors, such as Cdkn1a (or p21) and Cdkn2a (or p16), are play an important role in cell protection against DNA damage by directly interfering with CDKs and inducing cell cycle arrests.[31] One such example is cellular senescence induction in epithelial cells, where p21 can irreversibly stop the cell cycle upon extensive DNA damage as a protective mechanism against cancer development.[5] In immune cells, p21 can drive macrophage and dendritic cell differentiation during hematopoiesis,[32] can regulate apoptosis and DNA repair in neutrophils,[33] or can regulate the cell cycle of B cells.[34] Until now, the role of p21 in CD4$^+$ T cells has only been discussed in the context of inflammatory diseases, such as systemic lupus erythematosus.[18,35,36] Here, we describe for the first time the unknown functional role of p21 in CD4$^+$ T cells during CRC development.
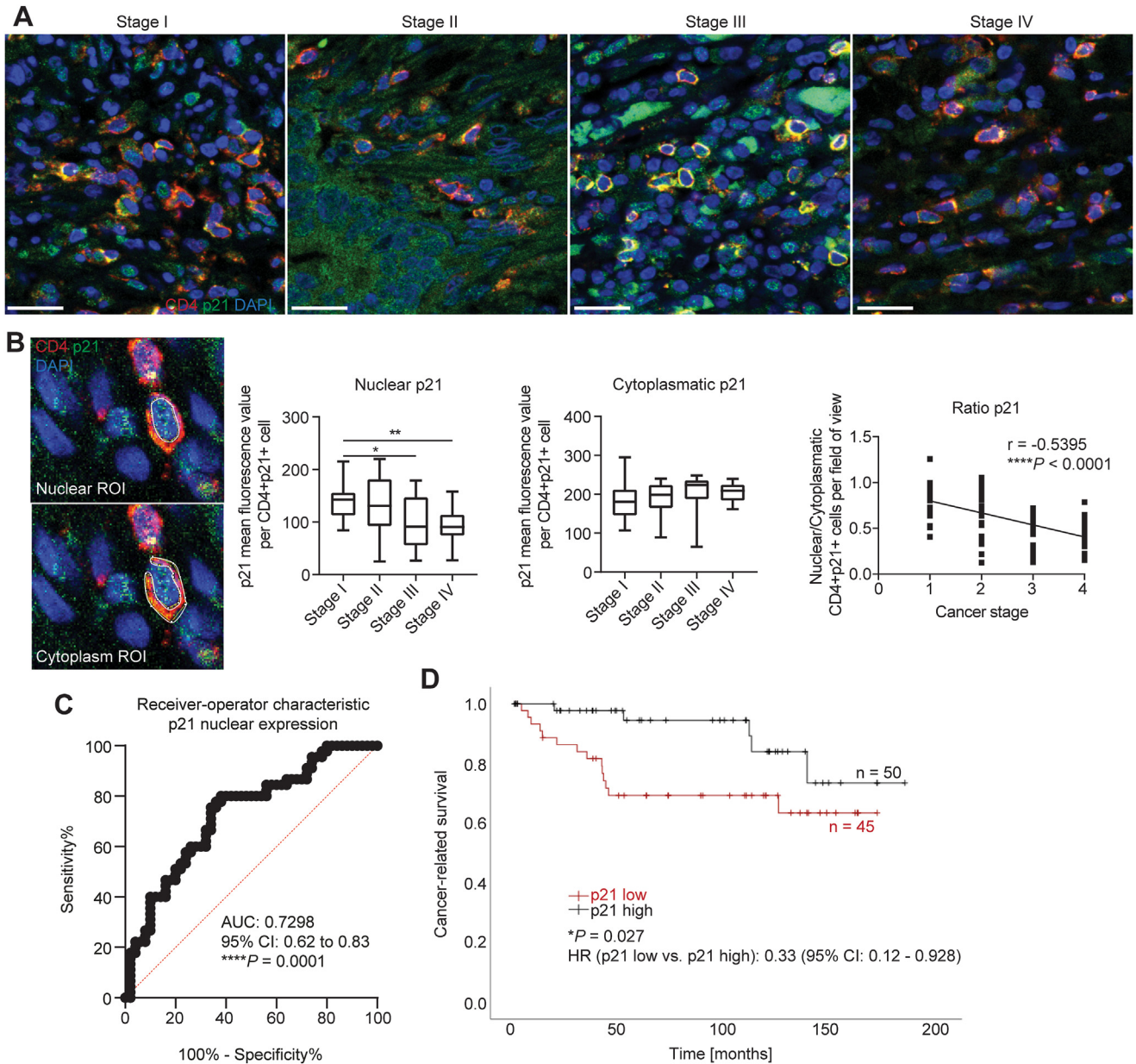
Figure 7. Prognostic value of p21 nuclear expression in CD4+ T cells. (*A*) Representative images show p21-expressing CD4+ T cells in patients with stage I to IV colorectal cancer. (*B*) Quantitative p21 expression in the nucleus and cytoplasm of CD4+ T cells infiltrated at the tumor site, after setting the region of interests (ROIs) (n = ≥18 patients/stage). The boxes indicate the 25th percentile (bottom border), median (center line), and 75th percentile (top border), and the whiskers show the maximum and minimum ranges. (*C*) Receiver operating characteristic curve using p21 nuclear expression in CD4+ T cells. p21 nuclear expression in patients with stages III and IV CRC compared with that of patients with stages I and II (AUC, area under the curve; CI, confidence interval). (*D*) Cancer-related survival of patients with low and high p21 nuclear expression in CD4+ T cells. The data are shown as the mean ± standard deviation. Significant differences are observed by using 1-way analysis of variance corrected with Tukey's multiple comparison test. Curves were plotted by using a simple linear regression model, and *r* values were calculated with the parametric Pearson's correlation. *$P \le .05$. **$P \le .01$, ****$P \le .0001$.

Our study showed that low or no p21 expression in CD4+ T cells increases tumor growth in animal models, whereas patients with CRC with low p21-expressing CD4+ T cells showed worse cancer-related survival than those with high levels of p21. We observed that p21-deficient T cells might impact the numbers of neutrophils found in the TME. This phenotype might be the result of decreased IFNγ and IL17A protein levels in immune cells from the TME, which could mediate neutrophil recruitment and trafficking at the tumor site.[37,38] Most interestingly, the cytotoxic potential of p21-deficient Th1 cells was significantly decreased in tumor mouse models. This phenotype was still present when normal p21-expressing CD8+ T cells were supplied. Various studies have reported the increased value of cytotoxic CD4+

T cells in the TME, no matter whether CD8^{+} T cells contribute or not to tumor cell killing.[39]

The loss of p21 in CD4^{+} T cells also affected cell maturation and CD27/CD28 costimulatory molecule expression, both in in vivo tumor models and in in vitro polarization experiments. We attribute these changes to the increased proliferation of p21^{−/−} T cells. Studies of human T cells have shown that after the first antigen encounter, naïve T cells respond and become central memory and effector cells.[40] Extensive exposure of the same antigen, however, leads to accumulation of exhausted T cells, such as TEMRA cells.[27] Common hallmarks of T-cell exhaustion can often be observed in CRC settings: exhausted T cells do not express CD27/CD28[41] but rather the inhibitory molecules CTLA4 and programmed cell death-1.[42] Furthermore, exhausted T cells show significant DNA damage, which reduces their effector function.[43–45] Interestingly, our results showed that p21 deficiency leads to exhaustion of Th1 cells, because the TME of Rag1^{−/−} mice reconstituted with p21^{−/−} CD4^{+} T cells had increased the relative numbers of effector/effector memory T cells that do not express CD27/CD28 costimulatory molecules. Our in vitro experiments have further shown increased DNA damage in p21^{−/−} Th1 cells compared with the control ones, which contributes to their exhaustion.

p21 expression was observed in the cell cytoplasm and nucleus of CD4^{+} T cells infiltrated in the TME in human and murine CRC samples. The functional role of p21 can vary depending on its localization: its expression in the nucleus is known to induce reversible (quiescence) or irreversible (senescence) cell cycle arrests and can promote DNA repair via proliferating cell nuclear antigen, whereas its translocation in the cell cytoplasm prevents apoptosis by directly interacting with the nuclear factor-κB (nuclear factor "κ-light-chain-enhancer" of activated B-cells) pathway.[46–49] When investigating B6/J Th1 cells, we found p21 expression was mostly observed in the cell nucleus.

Recent studies of various mammalian cell lines have demonstrated how important a certain level of p21 is during normal proliferation to mediate the naturally occurring DNA damage.[50,51] The duration and strength of its expression depends on the extent of damage. Therefore, we consider that p21 acts as a "gate keeper" before T cells enter the synthesis phase, ensuring that the DNA damage is not critical and that the necessary genes and proteins for effector function have been transcribed.

The importance of p21-mediated cell cycle arrest during the G1 phase was observed when Th1 cells were treated with CDK4/6 inhibitors. CDK4/6 inhibitors (abemaciclib, palbociclib, and ribociclib) are all able to target the formation of the CDK4/6–cyclin D complex, and directly reduce the phosphorylation of the Rb protein, therefore inducing cell cycle arrest.[52] Currently, CDK inhibitors are evaluated in clinical studies as potential therapeutics for the treatment of CRC.[9] Whereas the effect of CDK4/6 in cancer has been mostly related to the inhibition of cell cycle progression in cancer cells, only a limited number of studies have evaluated how CDK4/6 inhibitors affect adaptive immunity and especially T-cell function. For example, palbociclib

treatment on preexisting effector T cells of patients with metastatic breast cancer induced an increase in the relative numbers of circulating effector memory CD4^{+} and CD8^{+} T cells.[53] Similarly, treatment of CD8^{+} T cells with palbociclib increased the number of central memory cells in mice challenged with B16 melanoma cells, but had no effect on their cytotoxic function.[54] Therefore, understanding how CDK inhibitors affect not only tumor cells but also the effector function of T cells would result in an optimized therapy against CRC.

Although our experiments did not show any drastic changes in effector function or maturation of wild-type Th1 cells, p21-deficient ones were especially sensitive to palbociclib treatment, significantly increasing their cytotoxic potential, restoring memory phenotype, and preserving CD28 expression. To our knowledge, such effect of palbociclib on improving the cytotoxic function of exhausted Th1 cells has not been described until now. Ribociclib was also able to partially restore the cytotoxic potential of p21-deficient Th1 cells, but to a lesser degree compared with palbociclib. Abemaciclib, on the other hand, did not induce any changes in p21^{−/−} Th1 cells or even rather decreased the relative number of IFNγ^{+} T cells. Furthermore, among the 3 tested CDK4/6 inhibitors, abemaciclib treatment resulted in an increased rate of cell death in T cells and significantly reduced the number of cells the G0/G1 and G2/mitotic phase. We confirmed our flow cytometry results by Western blot, where abemaciclib markedly reduced the expression of phosphorylated Rb compared with palbociclib and ribociclib, indicating less to no proliferation.

Various studies showed that CDK4/6 inhibitors have different mechanisms of action.[55,56] For example, preclinical experiments demonstrated that the half maximum inhibitory concentration (IC50) differs among them: abemaciclib—IC50 of 2 nmol/L (CDK4) and 9.9 nmol/L (CDK6); palbociclib—IC50 of 9 to 11 nmol/L (CDK4) and 15 nmol/L (CDK6); and ribociclib—IC50 of 10 nmol/L (CDK4) and 39 nmol/L (CDK6). Furthermore, they have different binding properties as well: 93% to 98% for abemaciclib, ∼85% for palbociclib, and ∼70% for ribociclib.[57] Abemaciclib has also been shown to have an additional activity on CDK9, which is involved in cell proliferation. Therefore, based on the studies in the literature and the results of our own experiments, we conclude that abemaciclib has different mechanisms of action compared with ribociclib and palbociclib on cells, which seem to be independent from CDK4/6 inhibition.

T-cell infiltration in tumors from patients with CRC is usually considered a positive marker for overall survival.[58] Nevertheless, the type and effector potential of these cells also affects their outcome. Although Th1 and effector memory T cells are usually correlated to a better overall survival,[59] "bystander" and exhausted T cells can have negative effects on CRC development.[44] Our preliminary results also showed that patients with p21 high CD4^{+} T cells are less prone to cancer recurrence compared with those that had p21 low CD4^{+} T cells in the TME. p21 nuclear expression in CD4^{+} T cells could potentially be used as a prognostic marker for describing outcomes in patients with

CRC, even when CD4$^+$ T-cell numbers remain similar among tested samples (data not shown).

Overall, this study provides new insights on p21 function in CD4$^+$ T cells during their effector function against CRC. p21 loss directly affects IFNγ production of Th1 cells, whereas excessive proliferation leads to their exhaustion. Such cells are therefore less effective in tumor cell killing. Most interesting, patients with CRC who have low p21 expression in CD4$^+$ T cells are more predisposed to cancer relapse. Nevertheless, our preliminary studies on mouse models show that this phenotype can be restored by palbociclib, a CDK4/6 inhibitor that is already being explored in various clinical cancer trials as a direct inhibitor of cancer cell proliferation. We expect that our findings on the p21 function in CD4$^+$ T cells and the restorative potential of palbociclib will be translated into clinical therapies that will benefit patients with CRC. CDK4/6 inhibitors, such as palbociclib, could thereby act by directly targeting cancer cells and improving the antitumor immune response at the same time.

Supplementary Material

Note: To access the supplementary material accompanying this article, visit the online version of *Gastroenterology* at www.gastrojournal.org, and at https://doi.org/10.1053/j.gastro.2023.09.017.

References

1. World Health Organization. Cancer, 2022. Available at: https://www.who.int/news-room/fact-sheets/detail/colorectal-cancer.
2. La Vecchia S, Sebastian C. Metabolic pathways regulating colorectal cancer initiation and progression. Semin Cell Dev Biol 2020;98:63–70.
3. Kohrman AQ, Matus DQ. Divide or conquer: cell cycle regulation of invasive behavior. Trends Cell Biol 2017;27:12–25.
4. Cho KR, Vogelstein B. Genetic alterations in the adenoma–carcinoma sequence. Cancer 1992;70:1727–1731.
5. Kumari R, Jat P. Mechanisms of cellular senescence: cell cycle arrest and senescence associated secretory phenotype. Front Cell Dev Biol 2021;9:645593.
6. Nassour J, Martien B, Martin N, et al. Defective DNA single-strand break repair is responsible for senescence and neoplastic escape of epithelial cells. Nat Commun 2016;7:10399.
7. Zirbes TK, Baldus SE, Moenig SP, et al. Prognostic impact of p21/waf1/cip1 in colorectal cancer. Int J Cancer 2000;89:14–18.
8. **Oh HJ**, **Bae JM**, Wen XY, et al. p53 expression status is associated with cancer-specific survival in stage III and high-risk stage II colorectal cancer patients treated with oxaliplatin-based adjuvant chemotherapy. Br J Cancer 2019;120:797–805.
9. Thoma OM, Neurath MF, Waldner MJ. Cyclin-dependent kinase inhibitors and their therapeutic potential in colorectal cancer treatment. Front Pharmacol 2021;12:757120.
10. Galon J, Costes A, Sanchez-Cabo F, et al. Type, density, and location of immune cells within human colorectal tumors predict clinical outcome. Science 2006;313:1960–1964.
11. Masuda K, Kornberg A, Miller J, et al. Multiplexed single-cell analysis reveals prognostic and non-prognostic T cell types in human colorectal cancer. JCI Insight 2022;7:e154646.
12. Simoni Y, Becht E, Fehlings M, et al. Bystander CD8(+) T cells are abundant and phenotypically distinct in human tumour infiltrates. Nature 2018;557:575–579.
13. Zhang L, Yu X, Zheng LT, et al. Lineage tracking reveals dynamic relationships of T cells in colorectal cancer. Nature 2018;564:268–272.
14. Di J, Liu M, Fan Y, et al. Phenotype molding of T cells in colorectal cancer by single-cell analysis. Int J Cancer 2020;146:2281–2295.
15. Dinc Akbulut G, Ozkazanc D, Esendagli G. Th1 cells in cancer-associated inflammation. Turk J Biol 2017;41:20–30.
16. Knutson KL, Disis ML. Tumor antigen-specific T helper cells in cancer immunity and immunotherapy. Cancer Immunol Immunother 2005;54:721–728.
17. Montes CL, Chapoval AI, Nelson J, et al. Tumor-induced senescent T cells with suppressor function: a potential form of tumor immune evasion. Cancer Res 2008;68:870–879.
18. Arias CF, Ballesteros-Tato A, Garcia MI, et al. p21CIP1/WAF1 controls proliferation of activated/memory T cells and affects homeostasis and memory T cell responses. J Immunol 2007;178:2296–2306.
19. Deng C, Zhang P, Harper JW, et al. Mice lacking p21CIP1/WAF1 undergo normal development, but are defective in G1 checkpoint control. Cell 1995;82:675–684.
20. Mombaerts P, Iacomini J, Johnson RS, et al. Rag-1-deficient mice have no mature lymphocytes-B and lymphocytes-T. Cell 1992;68:869–877.
21. Neufert C, Becker C, Neurath MF. An inducible mouse model of colon carcinogenesis for the analysis of sporadic and inflammation-driven tumor progression. Nat Protoc 2007;2:1998–2004.
22. Zigmond E, Halpern Z, Elinav E, et al. Utilization of murine colonoscopy for orthotopic implantation of colorectal cancer. PLoS One 2011;6:e28858.
23. Becker C, Fantini MC, Neurath MF. High resolution colonoscopy in live mice. Nat Protoc 2006;1:2900–2904.
24. Kapoor V, Telford WG. Telomere length measurement by fluorescence in situ hybridization and flow cytometry. Methods Mol Biol 2004;263:385–398.
25. **Rosendahl P**, **Plak K**, Jacobi A, et al. Real-time fluorescence and deformability cytometry. Nat Methods 2018;15:355–358.
26. Pennock ND, White JT, Cross EW, et al. T cell responses: naive to memory and everything in between. Adv Physiol Educ 2013;37:273–283.
27. Larbi A, Fulop T. From "truly naive" to "exhausted senescent" t cells: when markers predict functionality. Cytometry Part A 2014;85a:25–35.

28. He GG, Siddik ZH, Huang ZF, et al. Induction of p21 by p53 following DNA damage inhibits both Cdk4 and Cdk2 activities. Oncogene 2005;24:2929–2943.

29. Lim S, Kaldis P. Cdks, cyclins and CKIs: roles beyond cell cycle regulation. Development 2013;140:3079–3093.

30. Eggersmann TK, Degenhardt T, Gluz O, et al. CDK4/6 inhibitors expand the therapeutic options in breast cancer: palbociclib, ribociclib and abemaciclib. BioDrugs 2019;33:125–135.

31. Karimian A, Ahmadi Y, Yousefi B. Multiple functions of p21 in cell cycle, apoptosis and transcriptional regulation after DNA damage. DNA Repair (Amst) 2016; 42:63–71.

32. Kramer JL, Baltathakis I, Alcantara OS, et al. Differentiation of functional dendritic cells and macrophages from human peripheral blood monocyte precursors is dependent on expression of p21 (WAF1/CIP1) and requires iron. Br J Haematol 2002;117:727–734.

33. Martin C, Ohayon D, Alkan M, et al. Neutrophil-expressed p21/waf1 favors inflammation resolution in *Pseudomonas aeruginosa* infection. Am J Respir Cell Mol Biol 2016;54:740–750.

34. Mullins MW, Pittner BT, Snow EC. CD40-mediated induction of p21 accumulation in resting and cycling B cells. Mol Immunol 1998;35:567–580.

35. Ballesteros-Tato A, Arias CF, Balomenos D. Cell cycle inhibitors in T cell tolerance and autoimmunity control. Inmunología 2007;26:184–192.

36. Darzynkiewicz Z, Juan G, Bedner E. Determining cell cycle stages by flow cytometry. Curr Protoc Cell Biol 2001, Chapter 8, Unit 8.4.

37. Akbay E, Koyama S, Dranoff G, et al. Interleukin-17A promotes lung tumor progression through neutrophil attraction to tumor sites and mediating resistance to PD-1 blockade. J Thorac Oncol 2017;12:S1996.

38. Bonville CA, Percopo CM, Dyer KD, et al. Interferon-gamma coordinates CCL3-mediated neutrophil recruitment in vivo. BMC Immunol 2009;10:14.

39. Perez-Diez A, Joncker NT, Choi K, et al. CD4 cells can be more efficient at tumor rejection than CD8 cells. Blood 2007;109:5346–5354.

40. Koch S, Larbi A, Derhovanessian E, et al. Multiparameter flow cytometric analysis of CD4 and CD8 T cell subsets in young and old people. Immun Ageing 2008;5:6.

41. **Lee SW**, **Choi HY**, Lee GW, et al. CD8$^+$ TILs in NSCLC differentiate into TEMRA via a bifurcated trajectory: deciphering immunogenicity of tumor antigens. J Immunother Cancer 2021;9:e002709.

42. Saleh R, Taha RZ, Toor SM, et al. Expression of immune checkpoints and T cell exhaustion markers in early and advanced stages of colorectal cancer. Cancer Immunol Immunother 2020;69:1989–1999.

43. Jiang W, He Y, He W, et al. Exhausted CD8+T cells in the tumor immune microenvironment: new pathways to therapy. Front Immunol 2020;11:622509.

44. Thoma OM, Neurath MF, Waldner MJ. T Cell Aging in patients with colorectal cancer-what do we know so far? Cancers (Basel) 2021;13:6227.

45. Zhao YJ, Shao QX, Peng GY. Exhaustion and senescence: two crucial dysfunctional states of T cells in the tumor microenvironment. Cell Mol Immunol 2020; 17:27–35.

46. Abbas T, Dutta A. p21 in cancer: intricate networks and multiple activities. Nat Rev Cancer 2009;9:400–414.

47. Lee JY, Kim HS, Kim JY, et al. Nuclear translocation of p21(WAF1/CIP1) protein prior to its cytosolic degradation by UV enhances DNA repair and survival. Biochem Biophys Res Commun 2009;390:1361–1366.

48. Li R, Hannon GJ, Beach D, et al. Subcellular distribution of p21 and PCNA in normal and repair-deficient cells following DNA damage. Curr Biol 1996;6:189–199.

49. Tillhon M, Cazzalini O, Dutto I, et al. p21CDKN1A and DNA repair systems: recent findings and future perspectives. In: Chen C, ed. New research directions in DNA repair. IntechOpen, 2013, Chapter 10. Available at: https://www.intechopen.com/chapters/44597.

50. Arora M, Moser J, Phadke H, et al. Endogenous replication stress in mother cells leads to quiescence of daughter cells. Cell Rep 2017;19:1351–1364.

51. **Barr AR**, **Cooper S**, **Heldt FS**, et al. DNA damage during S-phase mediates the proliferation-quiescence decision in the subsequent G1 via p21 expression. Nat Commun 2017;8:14728.

52. Corona SP, Generali D. Abemaciclib: a CDK4/6 inhibitor for the treatment of HR+/HER2- advanced breast cancer. Drug Des Devel Ther 2018;12:321–330.

53. Egelston C, Guo WH, Yost S, et al. Pre-existing effector T-cell levels and augmented myeloid cell composition denote response to CDK4/6 inhibitor palbociclib and pembrolizumab in hormone receptor-positive metastatic breast cancer. J Immunother Cancer 2021;9: e002084.

54. **Heckler M**, **Ali LR**, Clancy-Thompson E, et al. Inhibition of CDK4/6 Promotes CD8 T-cell Memory Formation. Cancer Discov 2021;11:2564–2581.

55. Braal CL, Jongbloed EM, Wilting SM, et al. Inhibiting CDK4/6 in breast cancer with palbociclib, ribociclib, and abemaciclib: similarities and differences. Drugs 2021; 81:317–331.

56. Marra A, Curigliano G. Are all cyclin-dependent kinases 4/6 inhibitors created equal? NPJ Breast Cancer 2019; 5:27.

57. Schettini F, De Santo I, Rea CG, et al. CDK 4/6 inhibitors as single agent in advanced solid tumors. Front Oncol 2018;8:608.

58. McMullen TPW, Lai R, Dabbagh L, et al. Survival in rectal cancer is predicted by T cell infiltration of tumour-associated lymphoid nodules. Clin Exp Immunol 2010; 161:81–88.

59. Pages F, Berger A, Camus M, et al. Effector memory T cells, early metastasis, and survival in colorectal cancer. N Engl J Med 2005;353:2654–2666.

Correspondence
Address correspondence to: Oana-Maria Thoma, PhD, Department of Medicine 1, Friedrich-Alexander-Universität Erlangen-Nürnberg, Hartmannstrasse 14, 91052 Erlangen, Germany. e-mail: oana-maria.thoma@uk-erlangen.de.

Conflicts of interest
The authors disclose no conflicts.

Data Availability
Data were generated by the authors and are available on reasonable request.

Supplementary Materials and Methods

In Vivo Colorectal Cancer Models

For the sporadic tumor model, murine carcinoma MC38 cells were injected in the submucosal layer of the colon. For the colitis-associated cancer model, 1 dose of AOM (Sigma-Aldrich) was injected intraperitoneally, followed by 1 cycle of DSS (MP Bio) in drinking water. $Rag1^{-/-}$ mice were also reconstituted by intraperitoneally injecting 2.5×10^6 of a mixture of $CD8^+$ (30%) and $CD4^+$ (70%) T cells $CD4^+$ T cells alone. T cells were isolated from the spleens of B6/J and $Cdkn1a^{-/-}$ ($p21^{-/-}$) mice using commercially available kits (Miltenyi Biotec).

The MC38 orthotopic model using palbociclib-treated memory T cells was performed as follows: First, $Cdkn1a^{-/-}$ mice were orthotopically injected with MC38 cells. Memory $CD4^+CD44^+$ T cells were isolated from spleens and mLNs of these mice (BD FACSAria II Flow Cytometer, BD Biosciences) and in vitro stimulated with α-CD3/α-CD28 for 24 hours. Before these cells were injected in MC38-bearing $Rag1^{-/-}$ mice, the activated $CD4^+CD44^+$ T cells were treated with palbociclib isothionate (Selleckchem) for 15 minutes at 37°C. We ensured that all palbociclib was removed by washing the cells with phosphate-buffered saline. As the control, littermates were injected with untreated, but only activated cells.

To evaluate immune cells infiltrated in the tumor microenvironment, we dissociated the tumor tissue using a mixture of collagenase D and deoxyribonuclease I. The cells obtained after the digestion were filtered through 40-μm filters. The recovered immune cells were then used for flow cytometric and enzyme-linked immunosorbent assay (ELISA) measurements.

Flow Cytometry Analysis

The cells were washed with fluorescence-activated cell sorter buffer containing Dulbecco's phosphate-buffered saline (Merck) plus 1% fetal bovine serum (Gibco). Cellular staining was then performed. For intracellular staining, the cells were fixed and permeabilized using the FoxP3 Transcription kit (Invitrogen) and then stained with the antibodies of interest (Tbet, Gata3, Rorγt, and FoxP3). For apoptosis detection, the AnnexinV Apoptosis Detection kit (eBioscience) was used. Cell proliferation assay was performed by using Cell Tracker Deep Red Dye (Thermo Fisher Scientific), as described in the manufacturer's protocol. To differentiate between Th1 and MC38 cells in our coculture experiments, forward and side scattering, along with CD4 staining, was used. MC38 cells were gated based on high forward scattering-A and side scattering-A, followed by $CD4^-$ expression.

MC38 Cell Death Analysis Using Incucyte

Palbociclib-treated and untreated Th1 cells were cocultured with MC38 cells for 24 hours in Incucyte Live-Cell Analysis System (Sartorius). MC38 cells were prestained with Cell Tracker Deep Red Dye (Thermo Fisher Scientific). Apoptosis was tracked by using Incucyte Caspase-3/7 Green Dye (Sartorius). The changes were observed using Incucyte S3 software (Sartorius). For accurate investigation of tumor apoptosis, the contribution of Cell Tracker Deep Red Dye fluorescence signal in the Caspase-3/7 Green Dye channel was corrected by 5%. MC38 tumor cell death has been calculated as (red + green area)/red area.

Real-Time Fluorescence Deformability Cytometry

An image of each cell was recorded together with the 3 fluorescence traces (FL1, FL2, and FL3), including peak positions. Cell images and fluorescence traces were stored and analyzed using ShapeOut software and Origin 2019b (OriginLab). p21 signals in each cell relative to the cytosolic Cell Tracker and the nuclear Ki67, relative peak positions were calculated: $position_{Cell\ Tracker} - position_{p21}$ and $position_{Ki67} - position_{p21}$. To test the colocalization of p21 and Ki67, $position_{p21} - position_{Cell\ Tracker}$ and $position_{Ki67} - position_{Cell\ Tracker}$, were analyzed. The 2-sample Kolmogorov-Smirnov test was then performed.

Histology and Immunostaining

Paraffin-embedded tissues from MC38 and AOM/DSS models were stained by using H&E. Tissue morphology was then evaluated by using a DMi4000B inverse microscope (Leica).

For immunohistochemistry staining, paraffin-embedded human and mouse tissues were first deparaffinized. After antigen retrieval (1x Antigen Retrieval solution, Dako), the slides were incubated with the Avidin/Biotin blocking kit (Vector Laboratories) and Protein Block solution (Dako). Tissue sections were incubated with the primary antibody diluted in Tris-buffered saline with 1% Tween 20 (Sigma-Aldrich) with 2% bovine serum albumin (Carl Roth). Secondary antibodies were then added, followed by staining with fluorescence dye for visualization. Finally, the cell nuclei were counterstained with 4′,6-diamidino-2-phenylindole, and the slides were mounted with Fluorescence Mounting Medium (Agilent). A list with the primary and secondary antibodies, as well as of the dyes can be found in Supplementary Table 3. The immunohistochemistry staining was measured by using a confocal microscope (TCS SP5, Leica) and analyzed using ImageJ software (National Institutes of Health), by investigating the area percentage stained with the antibody of interest related to the area percentage of 4′,6-diamidino-2-phenylindole.

For staining quantification of the human samples, 4 to 6 images per tissue sample were acquired. The analysis was done by randomly choosing 5 p21-expressing $CD4^+$ T cells from each image. A region of interest in ImageJ for cytoplasm and nuclear staining was set. The images were thresholded, and the mean fluorescence value for nuclear and cytoplasm p21 expression was determined.

For cell death detection in coculture experiments, Th1 cells were stained with Cell Tracker Green CMFDA Dye before being mixed with MC38 cells. After 24 hours, the cells were stained with propidium iodide.

Protein Isolation and Western Blot Analysis

The cells were homogenized in a buffer containing protease inhibitor cocktail (Merck) and M-PER Protein Extraction Reagent (Thermo Fisher Scientific). Then, 5 to 20 μg protein was separated on a 4% to 15% sodium dodecyl sulfate-polyacrylamide gel (Bio-Rad), and transferred to the nitrocellulose membrane (GE Healthcare). The membrane was blocked in Tris-buffered saline and Tween 20 plus 5% bovine serum albumin and incubated with the antibody of interest. The protein expression was assessed by using the Western Lightning Plus-ECL (PerkinElmer). As control, β-actin expression of all samples was analyzed. The antibodies used can be found in Supplementary Table 3.

Enzyme-Linked Immunosorbent Assay

ELISA protocols were conducted as described in the manufacturers' protocols. IFNγ, IL6, and IL17A ELISA kits (BioLegend) were used.

RNA Isolation, Complementary DNA Transcription, and Quantitative Real-Time Polymerase Chain Reaction

Cell suspensions were collected for DNA quantification as well. RNA isolation was performed by using the protocol and reagents from the MicoSpin Total RNA kit (PeqLab). Then, 20 to 50 ng RNA/20 μL was transcribed into complementary DNA by using the SCRIPT cDNA Synthesis kit (Jena Bioscience). The gene expression was analyzed by quantitative real-time polymerase chain reaction and normalized to hypoxanthine-guanine phosphoribosyltransferase. All used primers were ordered from Qiagen.

Receiver Operating Characteristic Curve Analysis

Receiver operating characteristic curve analysis was performed to determine the diagnostic ability of p21 nuclear expression in CD4$^+$ T cells in patients with CRC. p21 nuclear expression in patients with stage III to IV CRC was compared against the expression in patients with stage I and II. The receiver operating characteristic curve analysis was used to determine the area under curve. The cutoff value was calculated by using the maximized Youden's index, and estimates of sensitivity and specificity were derived. Finally, cancer-related survival was determined using Kaplan-Meier curves, based on the previously calculated cutoff value.
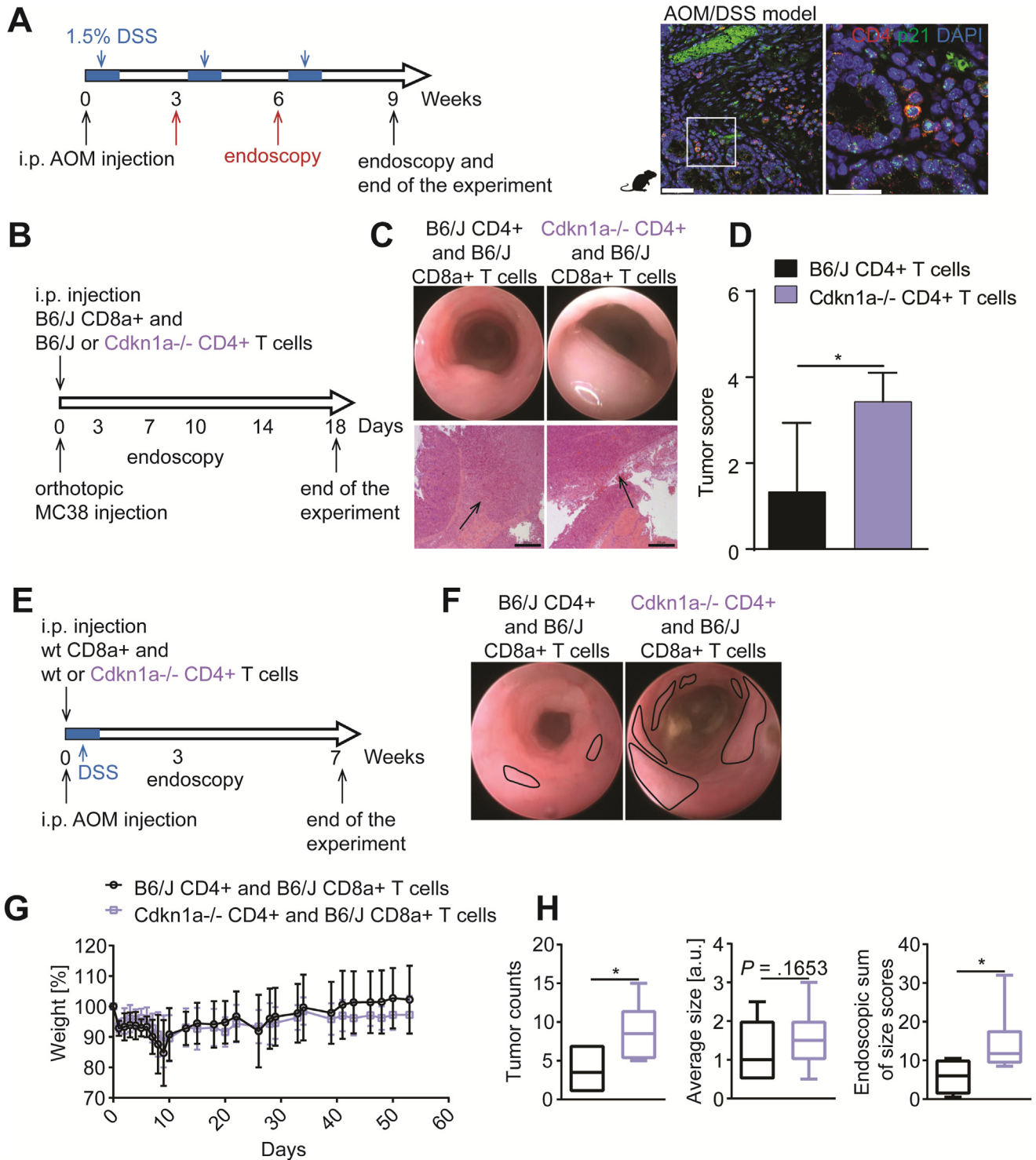
Supplementary Figure 1. p21 loss in CD4$^+$ T cells leads to increased tumor growth independent of cytotoxic CD8$^+$ T cells. (*A*) Schematic representation of the AOM/DSS model performed on B6/J mice, and immunohistochemistry images show p21 expression in CD4$^+$ T cells infiltrated in the TME (scale bar = 50 μm). i.p., intraperitoneal. (*B*) Schematic representation of the MC38 orthotopic model on Rag1$^{-/-}$ mice reconstituted with reconstituted with wild-type CD8$^+$ T cells and wild-type or p21-deficient CD4$^+$ T cells. (*C*) Representative endoscopic tumors and H&E images from these mice (scale bar = 100 μm). (*D*) Tumor scoring based on endoscopic measurements (n = ≥6 mice/group). (*E*) Schematic representation shows the used AOM/DSS model on Rag1$^{-/-}$ mice reconstituted with wild-type CD8$^+$ T cells and wild-type or p21-deficient CD4$^+$ T cells. (*F*) Representative endoscopic images show tumor growth in these mice. (*G*) Weight curve and (*H*) tumor size and number in Rag1$^{-/-}$ mice injected with B6/J or Cdkn1a$^{-/-}$ CD4$^+$ T cells, together with B6/J CD8$^+$ T cells. The boxes indicate the 25th percentile (bottom border), median (center line), and 75th percentile (top border), and the whiskers show the maximum and minimum ranges. The experiment shows n = ≥6 animals/group from 2 individual experiments. The data are shown as the mean ± standard deviation. Significant differences are observed by using the 2-tailed unpaired *t* test. *P ≤ .05.

A i.p. injection
wt or Cdkn1a-/- CD4+ T cells

B B6/J CD4+ T cells   Cdkn1a-/- CD4+ T cells

C B6/J CD4+ T cells   Cdkn1a-/- CD4+ T cells

D B6/J CD4+ T cells   Cdkn1a-/- CD4+ T cells

E Total number of live cells

F

G

H i.p. injection
wt CD8a+ and
wt or Cdkn1a-/- CD4+ T cells

I

J CD28+ cells
in the tumor
microenvironment
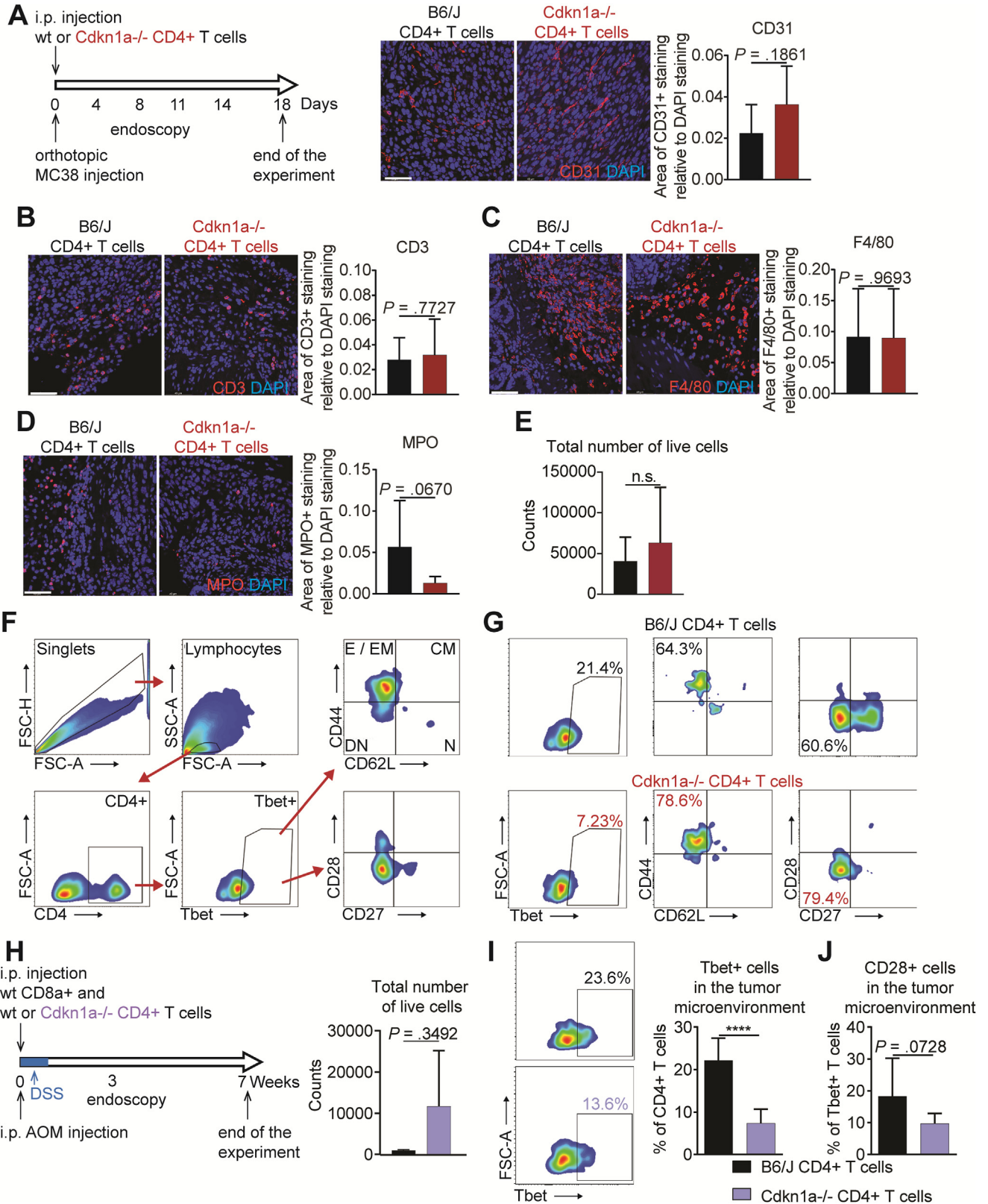
Supplementary Figure 2. Evaluation of the tumor microenvironment of Rag1$^{-/-}$ mice reconstituted with B6/J or Cdkn1a$^{-/-}$ CD4$^+$ T cells. (*A*) Schematic representation of the MC38 orthotopic model on Rag$^{-/-}$ mice reconstituted with wild-type or p21-deficient CD4$^+$ T cells and angiogenesis analysis by immunohistochemistry staining using CD31. DAPI, 4′,6-diamidino-2-phenylindole; i.p. intraperitoneal. (*B–D*) Immune cell infiltration in the TME as shown by F4/80, myeloperoxidase (MPO), and CD3 in the mice reconstituted with wild-type or p21$^{-/-}$ CD4$^+$ T cells (n = ≥4 samples/group). (*E*) Total number of live cells evaluated from the TME of Rag1$^{-/-}$ mice reconstituted with B6/J or p21$^{-/-}$ CD4$^+$ T cells. (*F*) Gating strategy for immune cell infiltration in the TME, as measured by flow cytometry. E/EM represents the effector/effector memory population; CM, the central memory Tbet$^+$ T cells; CD62L$^-$CD44$^-$ population is marked as DN, and N marks the naïve T cells. FSC, forward scatter; SSC, side scatter. (*G*) Representative flow cytometry plots show Tbet$^+$, effector/effector memory, and CD27$^-$CD28$^-$ Tbet$^+$ T cells from the TME of Rag$^{-/-}$ mice reconstituted with wild-type or p21-deficient CD4$^+$ T cells and exposed to the MC38 orthotopic model. (*H*) Schematic representation shows the AOM/DSS model used on Rag$^{-/-}$ mice reconstituted with wild-type CD8$^+$ T cells and wild-type or p21-deficient CD4$^+$ T cells and total number of live cells, as shown by flow cytometry data. (*I*) Representative flow cytometry gating and Tbet$^+$ infiltration from the tumor microenvironment of these mice, as shown by flow cytometry data. (*J*) CD28 expression in Tbet$^+$ T cells from the TME of Rag1$^{-/-}$ mice reconstituted with wild-type or p21-deficient CD4$^+$ T cells and exposed to the AOM/DSS model. The experiment shows n = ≥6 animals/group from 2 individual experiments. The data are shown as the mean ± standard deviation. Significant differences are observed by using 2-tailed unpaired *t* test or 2-way analysis of variance corrected with Šidák's multiple comparison test. *P≤.05.
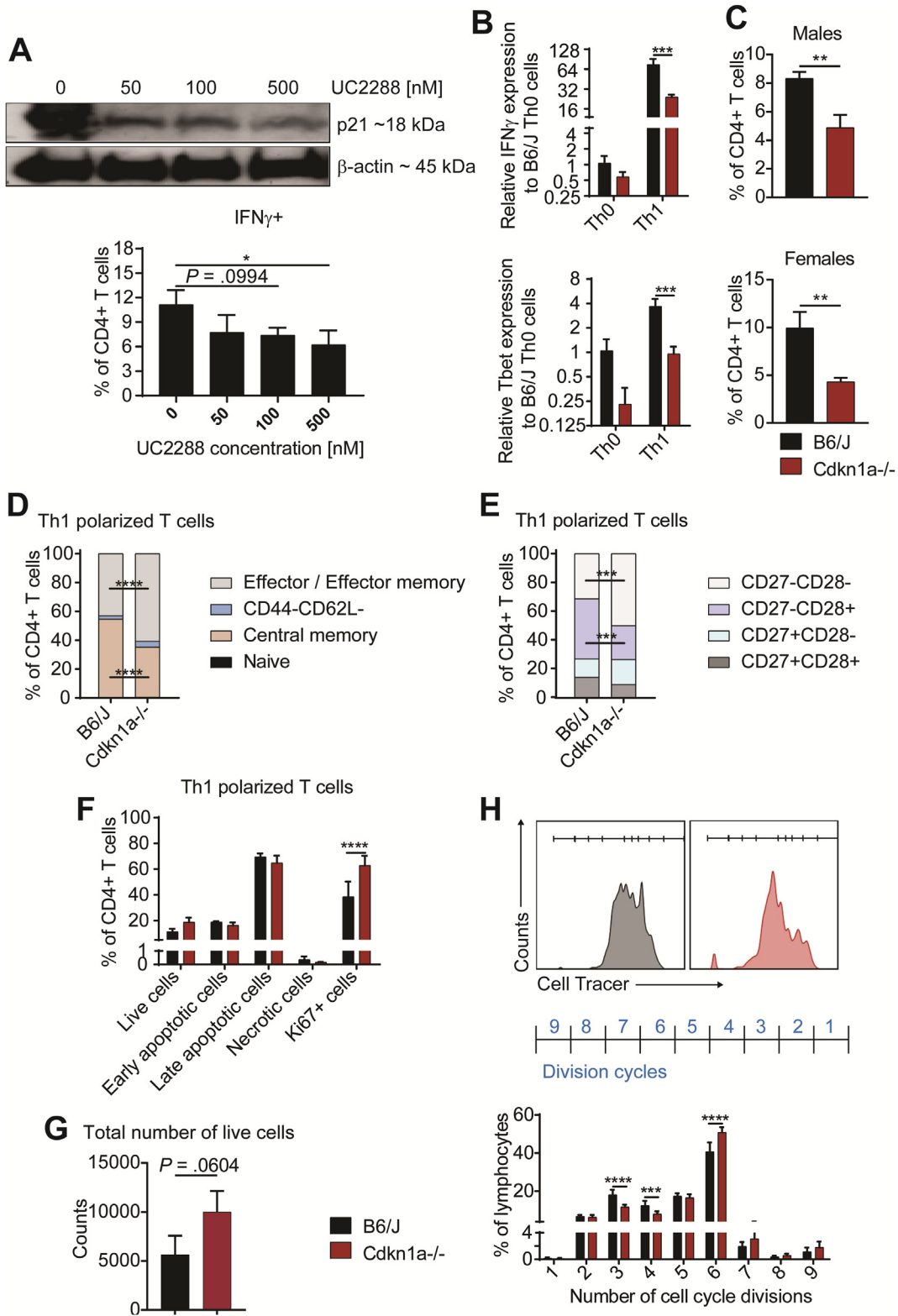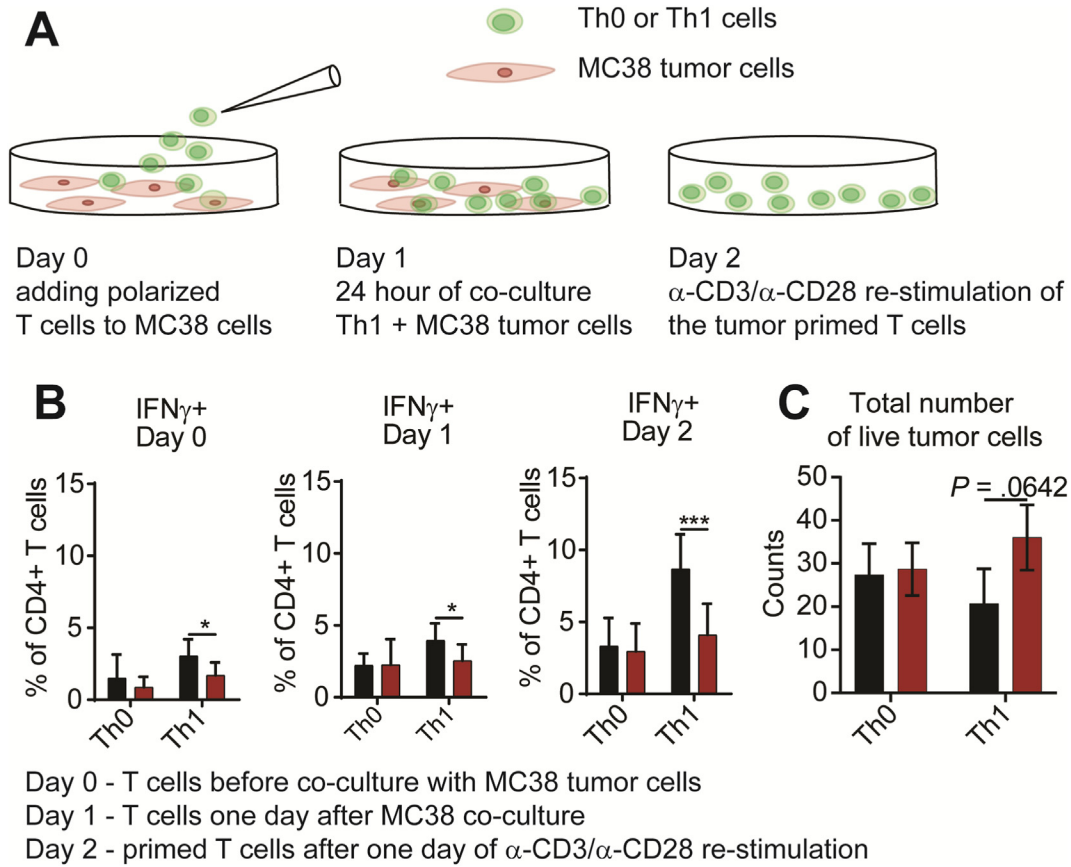
Supplementary Figure 4. Response to p21-deficient Th1 cells to MC38 exposure. (*A*) Schematic representation of the MC38-Th1 T-cell coculture experiments. Th0, naïve T-helper cells. (*B*) IFNγ expression before coculture, after MC38 cell priming, and 1 day after in vitro restimulation as shown by flow cytometry. (*C*) Flow cytometry measurements show total number of live tumor cells. The experiment was repeated 3 times. Data show cumulative results with n = ≥6 replicates/group. The data are shown as the mean ± standard deviation. Significant differences are observed using 2-way analysis of variance corrected with Šidák's multiple comparison test. *P≤.05, **P≤.01, ***P≤.0001.

Supplementary Figure 3. Increased proliferation of Cdkn1a$^{-/-}$ Th1 cells contributes changes in T-cell maturation and expression of the CD28 costimulatory molecule. (*A*) Western blot shows p21 reduction in in vitro polarized Th1 cells from B6/J mice in response to UC2288, a p21 inhibitor. p21 inhibition also reduces the relative numbers of IFNγ$^+$ T cells in a concentration-dependent manner (n = ≥2 replicates/group, experiment repeated 2 times). (*B*) IFNγ and Tbet expression determined by quantitative real-time polymerase chain reaction. Th0, naïve T-helper cells. (*C*) Flow cytometry data show the relative numbers of IFNγ$^+$ T cells in Th1 polarized from male and female B6/J or Cdkn1a$^{-/-}$ mice (n = ≥3 replicates/group). (*D* and *E*) CD27/CD28 expression of in vitro Th1 polarized T cells from control and p21-deficient mice. (*F* and *G*) Proliferation, cell death, and the total number of live cells of B6/J and Cdkn1a$^{-/-}$ Th1 cells, as shown by the flow cytometry data. Each experiment was performed at least 3 times with n = 3 replicates/group. (*H*) Representative data of Cell Tracker spectra showing in vitro Th1 proliferation from B6/J (black) and Cdkn1a$^{-/-}$ (red), as measured by flow cytometry data. Relative number of Th1 cells in various cell division states (*t* = 5 days of stimulation, n = 3 replicates/group). The data are shown as the mean ± standard deviation. Significant differences are observed by using 2-tailed unpaired *t* test or 2-way analysis of variance corrected with Šidák's multiple comparison test. *P ≤ .05. **P ≤ .01, ***P ≤ .001, ****P ≤ .0001.
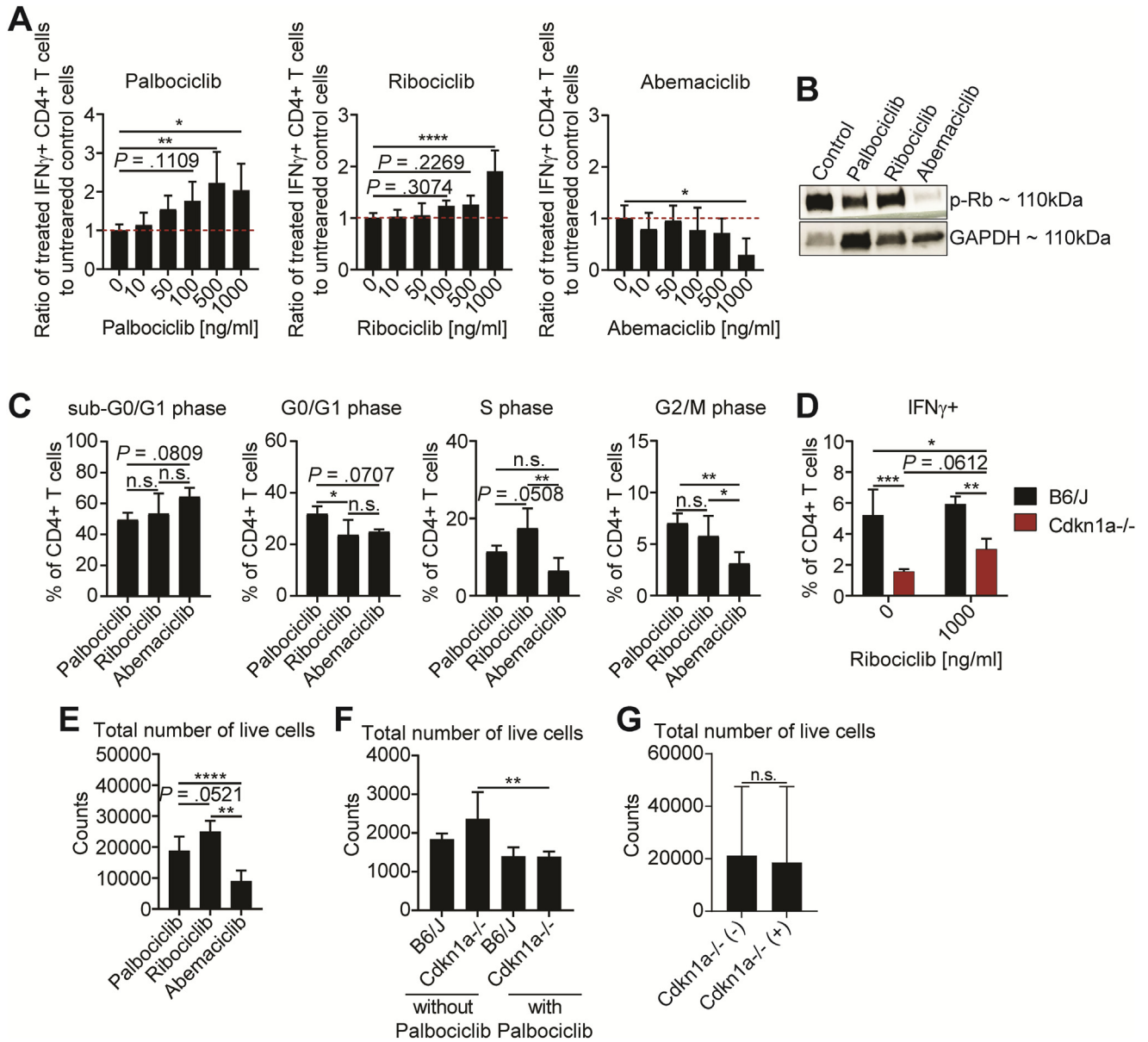
Supplementary Figure 5. Th1 cell function can be restored by CDK4/6 inhibitors palbociclib and ribociclib, but not abemaciclib. (A) Relative numbers of IFNγ^+ T cells of in vitro Th1 polarized cells from Cdkn1a$^{-/-}$ mice, after palbociclib, ribociclib, or abemaciclib treatment (n = ≥4 replicates/group, from 2 independent experiments), as shown by flow cytometry. (B) Western blot shows expression of phosphorylated Rb (p-Rb) after treatment with different CDK4/6 inhibitors. Glyceraldehyde-3-phosphate dehydrogenase (GAPDH) protein expression was used as the control. (C) Cell cycle phases in Cdkn1a$^{-/-}$ Th1 cells treated with palbociclib, ribociclib, or abemaciclib, as shown by flow cytometry. (D) Relative numbers of cells of IFNγ^+ T cells after ribociclib treatment of control and p21$^{-/-}$ CD4$^+$ T cells (n = 3 replicates/group). (E) Total number of live cells in after treatment of Cdkn1a$^{-/-}$ CD4$^+$ T cells with CDK4/6 inhibitors. (F) Number of total live tumor cells after coculture of MC38 with treated and untreated Th1 cells from B6/J and Cdkn1a$^{-/-}$ cells. (G) Total number of immune cells from the TME of Rag1$^{-/-}$ mice reconstituted with palbociclib-treated and untreated CD4$^+$ T cells, as shown by flow cytometry. The data are shown as the mean ± standard deviation. Significant differences are observed by using 2-tailed unpaired t test, 1-way analysis of variance corrected with Tukey's multiple comparison test, or 2-way analysis of variance corrected with Šidák's multiple comparison test. n.s., not significant; *$P \leq$ .05, **$P \leq$ .01, ****$P \leq$ .0001.

Supplementary Table 1. Patient and Colorectal Cancer Characteristics

Characteristics	Samples (n)	Mean age (years)	Men n (%)	Women n (%)
Stage				
I	18	69.5	12 (66.7)	6 (33.3)
II	32	68.9	19 (59.3)	13 (40.7)
III	24	68.1	16 (66.7)	8 (33.3)
IV	21	62.7	11 (52,4)	9 (47.6)
Classification				
R0	76	68.4	46 (60.5)	30 (39.5)
R1	10	67.5	7 (70)	3 (30)
R2	9	59.5	5 (55.5)	4 (45.5)
Location				
Ascending colon	21	67.8	10 (47.6)	11 (52.4)
Descending colon	8	68.8	6 (75)	2 (25)
Transverse colon	9	65.5	6 (66.7)	3 (33.3)
Sigmoid colon	36	68.3	28 (77.8)	8 (22.2)
Rectum	7	82	0 (0)	7 (100)
Cecal	11	68.6	4 (36.4)	7 (63.6)
Hepatic flexure	3	70	0 (0)	3 (100)

Supplementary Table 2. List of Stimulants Used for In Vitro CD4$^+$ T-Cell Experiments

Stimulant	Provider	Article number	Working concentration
Cell Stimulation Cocktail (500x)	Thermo Fisher Scientific	00-4970-93	1:500
InVivoMAb anti-mouse CD28	BioXCell	BE0015-1	10 μg/mL
InVivoMAb anti-mouse CD3e	BioXCell	BE0001-1	10 μg/mL
InVivoMab anti-mouse IL4	BioXCell	BE0199	5 μg/mL
Palbociclib (PD0332991) isothionate	Selleckchem	S1579	10–1000 ng/mL
Recombinant mouse IL12	R&D Systems	419-ML-010	10 μg/mL
UC2288, p21 inhibitor	Abcam	ab146969	10–500 nmol/L
Abemaciclib	Selleckchem	S5716	10–1000 ng/mL
Palbociclib	Selleckchem	S1579	10–1000 ng/mL
Ribociclib	Selleckchem	S7440	10–1000 ng/mL

Supplementary Table 3. Antibodies Used for Flow Cytometry, Immunohistochemistry, and Western Blot

Reactivity	Antigen	Company	Method
Mouse	Alexa Fluor 488 donkey IgG antibody	BioLegend	FACS
Mouse	Alexa Fluor 555 rat	Thermo Fisher Scientific	IHC
Mouse	Annexin V	BioLegend	FACS
Mouse	β-Actin	Abcam	WB
Mouse	Biotin CD28	BioLegend	FACS
Mouse	CD16/CD32	eBioscience	FACS
Mouse	CD25 PE	eBioscience	FACS
Mouse	CD4 APC	Miltenyi Biotec	FACS
Mouse	CD4 PE/Cy7	BioLegend	FACS
Mouse	CD4 primary antibody	Thermo Fisher Scientific	IHC
Human	CD4 primary antibody	Abcam	IHC
Mouse	CD62L PE	Invitrogen	FACS
Mouse	CD8a BV510	BD Bioscience	FACS
Mouse	Cleaved caspase-3 primary antibody	Cell Signaling	IHC
Mouse/human	DAPI	Sigma-Aldrich	FACS, IHC
Mouse	FoxP3 Pacific Blue	Invitrogen	FACS
Mouse	Gata3 FITC	Miltenyi Biotec	FACS
Mouse	IFNγ APC	Invitrogen	FACS
Mouse	Ki67 Pacific Blue	BioLegend	FACS
Mouse	Ki67 primary antibody	Abcam	IHC
Mouse	Mouse IgG HRP-linked secondary antibody	Cell Signaling	WB
Mouse/human	Mouse IgG secondary antibody	Invitrogen	IHC
Mouse	MPO primary antibody	Abcam	IHC
Mouse	p21	Boster Biological Technology	FACS, IHC, WB
Human	p21 primary antibody	Abcam	IHC
Mouse/human	PI staining solution	Invitrogen	FACS
Mouse	PNA FISH probe	Panagene	FACS
Mouse	Rabbit IgG HRP-linked secondary antibody	Cell Signaling	WB
Mouse/human	Rabbit IgG secondary antibody		IHC
Mouse	Rat IgG HRP-linked secondary antibody	Cell Signaling	WB
Mouse/human	Rat IgG secondary antibody	BD Bioscience	IHC
Mouse	Rorγt APC	Invitrogen	FACS
Mouse	Streptavidin Brilliant Violet 650	BioLegend	FACS
Mouse/human	Streptavidin, Dylight 488	Invitrogen	IHC
Mouse/human	Streptavidin, Dylight 550	Invitrogen	IHC
Mouse	CD4 SuperBright 600	eBioscience	FACS
Mouse	Tbet PerCP/Cy5.5	Invitrogen	FACS

Supplementary Table 3. Continued

Reactivity	Antigen	Company	Method
Mouse/human	TSA Cyanine 3 System	PerkinElmer	IHC
Mouse/human	TSA Fluorescein System	PerkinElmer	IHC

APC, allophycocyanin; DAPI, 4′,6-diamidino-2-phenylindole; FACS, fluorescence-activated cell sorter; FISH, fluorescence in situ hybridization; FITC, fluorescein isothiocyanate; HRP, horseradish peroxidase; Ig, immunoglobulin; IHC, immunohisto-chemistry; MPO, myeloperoxidase; PE, phycoerythrin; PI, propidium iodide; PNA, peptide nucleic acid; PerCP peridinin-chlorophyll-protein complex; WB, Western blot.